River ice phenology and thickness from satellite altimetry: Potential for ice bridge road operation and climate studies

Elena Zakharova[1,2], Svetlana Agafonova[3], Claude Duguay[4,5], Natalia Frolova[3], Alexei Kouraev[6]

1. Institute of Water Problems of Russian Academy of Science, Moscow, Russia

2. EOLA, Toulouse, France

3. Moscow State University, Moscow, Russia

4. University of Waterloo, Waterloo, Canada

5. H2O Geomatics, Waterloo, Canada

6. LEGOS, Université de Toulouse, CNES, CNRS, IRD, UPS Toulouse, France

Abstract

River ice is an important component of the cryosphere. Satellite monitoring of river ice is a rapidly developing area of scientific enquiry which has wide-ranging implications for climate, environmental, and socio-economic applications. Spaceborne radar altimetry is widely used for monitoring river water regimes, however its potential has not been demonstrated yet for the observation of river ice processes and properties. Using Ku-band backscatter measurements from the Jason-2 and -3 satellite missions (2008-2019), we demonstrate for the first time the potential of radar altimetry for the retrieval of river ice phenology dates and ice thickness. Altimetric measurements are shown to be sensitive enough to detect the first appearance of ice and the beginning of thermal breakup on the Lower Ob River (Western Siberia). Uncertainties in the retrieval of ice event timing are within the 10-day repeat cycle of Jason-2/3 for 88–90% of the cases analysed. River ice thickness retrievals from backscatter measurements via empirical relations with in-situ observations are within root mean square errors of 0.07-0.18 m. One of the novel applications of radar altimetry is in the prediction of ice bridge road operations, which is demonstrated herein. We show that the dates of ice road opening in Salekhard City can be predicted with an accuracy of four days. Uncertainties in the prediction of dates of ice road closure are three days, with the lead time varying from four days (for late breakup start) to 22 days (for early breakup start).

1 Introduction

River ice is a major component of the cryosphere. It affects an extensive portion of the hydrologic system in the Northern Hemisphere where seasonal ice impacts 58% of the total river length (Prowse et al., 2007). Hence monitoring the interannual variability and trends of river in response to climate is important for many environmental and societal applications. River ice plays a key role in the functioning of aquatic and riparian ecosystems (Prowse, 2001) and contributes to the erosion of channels and banks (Ettema, 2002) as well as the transport of sediments (Beltaos et al., 2018). River ice affects streamflow via the withdrawal (immobilisation) of part of the water during freeze-up and consequent release during breakup. In addition, ice jams on rivers can cause catastrophic flooding (Beltaos et al., 2013). From socio-economic and cultural perspectives, river ice affects the operation of hydropower stations as well as construction and navigation activities. In arctic regions, frozen rivers provide a unique transportation infrastructure for the movement of goods and people via winter ice roads and provide local populations with access to fishing and hunting/trapping grounds and, in some cases (e.g. Central Yakutia, Russia), to

freshwater. However, operational monitoring of ice cover on northern rivers is difficult due site accessibility. Moreover, ice conditions can be unsafe for people who perform in-situ measurements, especially at the beginning or end of the ice season. Therefore, satellite remote sensing has been proposed as an alternate tool, or complement, to ground-based measurements, allowing for the characterisation of river ice properties and processes at spatial and temporal resolutions suitable for addressing various scientific and operational requirements (Duguay et al., 2015).

Indeed, satellite-borne instruments provide observational capabilities to map and monitor many river ice parameters. For example, optical sensors such as the Moderate Resolution Imaging Spectroradiometer (MODIS) and the Advanced Very High-Resolution Radiometer (AVHRR) have been used to map river ice extent and phenology - freeze-up and breakup dates (Pavelsky and Smith, 2004; Chaouch et al., 2014; Chu and Lindenschmidt, 2016; Muhammad et al., 2016; Cooley and Pavelsky, 2016; Beaton et al., 2019). However, the presence of extensive cloud cover for many months of the year and low solar illumination conditions, particularly during the freeze-up period, are limiting factors for monitoring river ice at high latitudes using optical sensors. Active sensors operating in the microwave region of the electromagnetic spectrum are weather independent and provide a spatial resolution higher than that of the MODIS and AVHRR instruments. Synthetic aperture radar (SAR) imaging systems, in particular, have been used to monitor river ice phenology (e.g. Unterschultz et al., 2009; Mermoz et al., 2009; Sobiech et al., 2013; Sun and Trevor, 2018), deformation (Unterschultz et al., 2009), and classification of ice types (e.g. Chu and Lindenschmidt, 2016). Comprehensive reviews on remote sensing of lake and river ice can be found in Jeffries et al. (2005) and Duguay et al. (2015).

Ice thickness (Hice) is another parameter which is of particular interest for operational purposes, such as public safety, ice road service, ice jam forecasts, and mitigation. Passive microwave and thermal satellite instruments have shown potential for the retrieval of ice thickness for large lakes (Kang et al., 2014; Duguay et al., 2002, 2015; Gunn et al., 2015; Kheyrollah Pour et al., 2017). However, the spatial dimension of rivers, notably the width of channels, limits the application of these instruments as they only provide coarse spatial resolution (km to tens of km spatial resolutions). A few studies have used SAR images with high, 10-25 m, spatial resolutions to estimate river ice thickness (Unterschultz et al., 2009; Mermoz et al., 2014, Zhang et al., 2019), mainly through the establishment of statistical relations between backscatter and in-situ ice thickness measurements. However, these SAR-based methods have been limited to the estimation of ice thickness for short time periods (one or a few ice seasons) and small sections of rivers, primarily due to limited access to SAR imagery in years prior to the launch of the Sentinel-1A/B missions (since 2014) of the European Space Agency (ESA). Altimetric radars represent an excellent alternative or complement to SAR satellites. Satellite altimeters also provide relatively high spatial resolution (200-400 m) and are as well weather-independent instruments with a long history of observations starting in the mid 1980s. Radar altimeters have largely been used for monitoring water levels of inland waterbodies and water courses starting at 100-m in width (Michailovsky et al., 2012). Radar altimeter data products are freely accessible via portals operated by the French space agency (CNES: Centre national d'études spatiales) and ESA; data can be routinely and quickly processed over large areas for relatively long time periods.

Radar signals incident upon the Earth's surface are modified according to the physical properties of surface materials. Similar to imaging SAR systems, the signal recorded by radar altimeters can be interpreted as a function of changes in surface properties, and the backscatter coefficient (ratio between power of emitted and received signal) can be used to characterize surface state within a radar footprint. Radar backscatter from freshwater ice depends on the radar configuration (radar type, operating frequency, viewing geometry, polarisation) and on material properties such as ice thickness, layering, air bubble inclusions, liquid water content, surface roughness and snow on ice (Ulaby et al., 1986; Duguay et al., 2002; Leconte et al., 2009; Atwood et al., 2015; Gunn et al., 2015;

Antonova et al., 2016; Gunn et al., 2018). The potential of altimetric radars has already been demonstrated for the monitoring ice phenology dates of large Eurasian lakes (Kouraev et al., 2007, 2015) and for the estimation of ice thickness on large northern lakes in Canada (Beckers et al., 2017; Duguay et al., 2018). However, radar altimeters have not been used to date for monitoring the ice regime of rivers. Therefore, for the first time, we demonstrate the application of radar altimetry for monitoring the interannual variability of river ice phenology and ice thickness along a 400 km stretch of the Ob River (Siberia, Russia).

This paper describes the development and validation of algorithms for the retrieval of river ice phenology dates and ice thickness and the use of these products for the prediction of ice bridge road operations at Salekhard City on the Ob River. For this purpose, data from two altimetric satellite missions, Jason-2 and Jason-3, were selected for two reasons: 1) they provide the best temporal resolution (10 days) amongst altimetric missions; and 2) the lifetime of this series of satellites provides observations on the same orbit, starting in 1992 with the Topex/Poseidon and continues nowadays with the Sentinel-6 mission (launched in November 2020), which is offering an interesting perspective for a follow-up investigation on the response of river ice on the Ob to a changing Arctic climate.

2 Study Region

The study was conducted over an area that encompasses the lower reaches of the Ob River (Siberia, Russia). The Ob River drains the Western Siberian Plain and is the third largest river in the Arctic Ocean watershed, with a mean annual flow of 406 km^3 (Zakharova et al., 2020). The lower reaches of the Ob River extend for approximately 800 km and begin at the confluence of the Ob and the Irtysh rivers at 61.08°N (Figure 1). The reaches are characterised by a particularly wide floodplain (up to 50 km) and the presence of numerous branches. The easternmost channel is the main, largest branch, called the Big Ob. The second largest branch delineates the flood plain from the west. The Ob River watershed is one of the largest peat bog systems in the world (Zakharova et al., 2014), and many settlements, which are located on the high terraces of the two main branches, have limited interconnection and access to supplies. The main branches of the river are navigable; however, they are covered by ice for seven months of the year. In winter, when bogs are frozen, local communities intensify their socio-economic activities by constructing winter roads and ice bridges over river crossings. River ice observations on the Ob are sparse and taken only at a few gauging stations dedicated to water level monitoring. In this study, we selected a section of the lower reaches of the Ob River located between two large administrative centres (Salekhard and Khanty-Mansyisk).

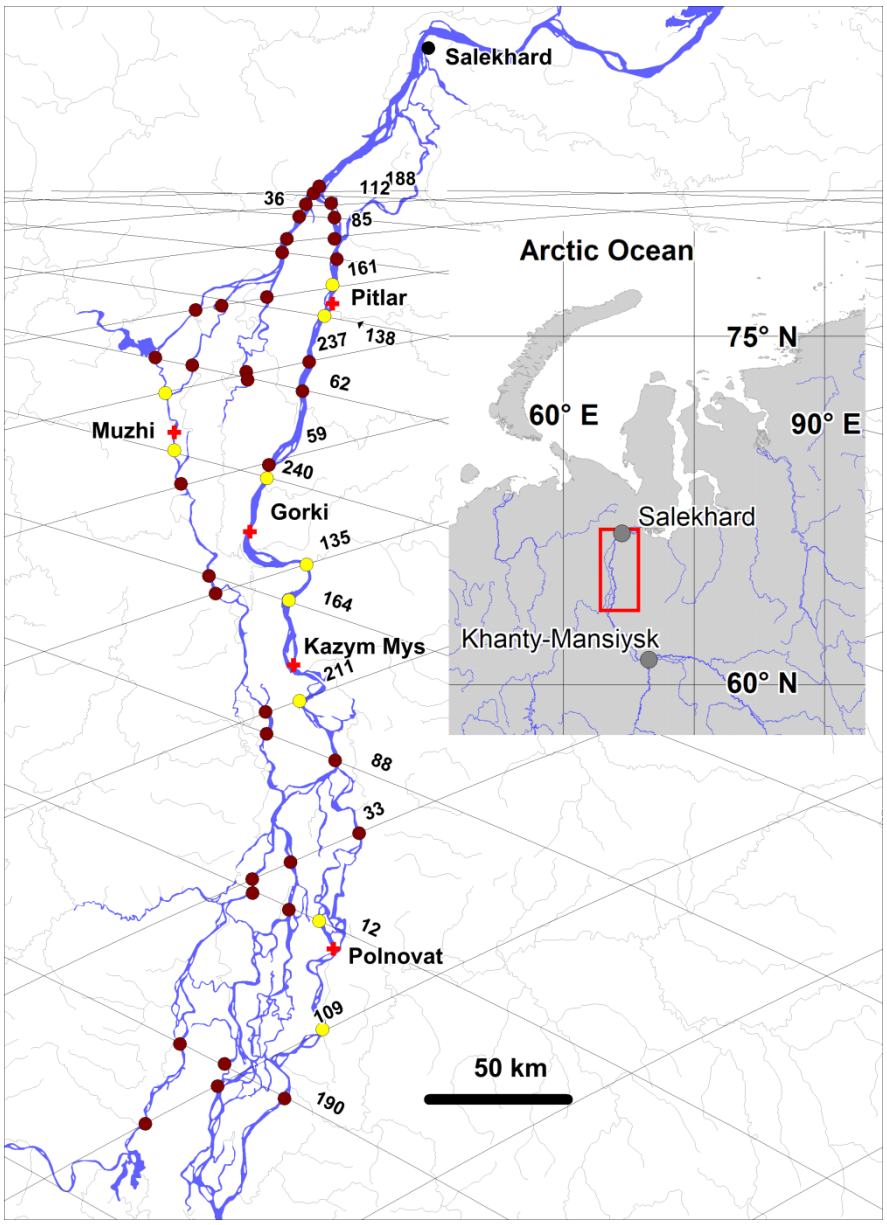

Figure 1. The lower reaches of the Ob River and location of the virtual (circles) and gauging (red crosses) stations. Stations from training set are shown as yellow circles. Jason-2 and -3 satellite tracks numbers are also provided at river crossings. The main map is produced using public The World Bank data (https://datacatalog.worldbank.org/dataset/major-rivers-world).

3 Data

3.1 In-situ data and ice regime at studied river reaches

The Russian Hydrometeorological Service monitors ice at all gauging stations measuring water level. There are five water level gauging stations in the studied Ob River reach (Figure 1; Table 1). Four stations (Polnovat, Gorki, Kazym-Mys, and Pitlar) are located on the main branch of the Ob River, and one station (Muzhi) provides observations on the secondary channel called the Small Ob River.

Table 1. Gauging stations in the lower reaches of the Ob River, including information on distance from the river mouth, beginning of observation periods, and periods with data gaps in observation records at stations.

River- station	Distance from mouth (km)	Beginning of observation period	Data gap in observation record
Ob – Polnovat	702	1970	
Ob – Gorki	487	1935	
Small Ob – Muzhi	463	1933	
Ob – Kazym Mys	551	1979	1988 –2003
Ob – Pitlar	386	1979	1990 – 2005

The standard protocol of river ice monitoring at the gauging stations involves: 1) daily visual observations of ice presence/absence and ice type/events; and 2) three to four times per month measurements of ice thickness and on-ice snow depth. Ice thickness is measured by drilling a single hole using an ice auger. Snow depth corresponds to an average value calculated from three snow-depth measurements located around the hole.

According to in-situ observations at the gauging stations, ice formation begins between 23 and 27 October. In the last 20 years, the earliest and latest records are 1 October and 18 November, respectively. At the studied river reaches, ice cover forms quickly, typically within just 2-3 days from appearance of first ice. However, in 15% of the cases, full freeze-up (from ice onset to complete freeze-over) takes up to 10 days. Ice grows rapidly during the first month of the ice season, and river ice reaches a thickness of 0.23-0.30 m already by the end of November. Towards the end of the ice growth period (March-April), the thickness of the ice cover is 0.80-1.0 m on average (maximum of 1.50 m). Snow depth on the ice surface varies from 0.09-0.13 m in November to 0.30-0.50 m in April. The temporal dynamics of ice growth on the large linear channel sections is similar throughout the studied reaches (Fig. 2a). However, in the south of the region, the ice thickness is 0.07 to 0.20 m less than in the north. Climate change has affected river ice in the Canadian Arctic (Prowse et al., 2011b) and the European part of Russia (Agafonova and Vasilenko, 2020), but has not yet resulted in a significant change in the ice regime of the entire lower Ob River.

Mann-Kendall tests performed on ice time series with complete records (Polnovat, Gorki and Muzhi; see Table 1) reveal that long-term trends in ice onset dates are occurring significantly later (0.05 level) only at the Polnovat station, while maximum ice thicknesses have become significantly thinner (0.05 level) at both the Gorki and Muzhi stations (Figure 2b).

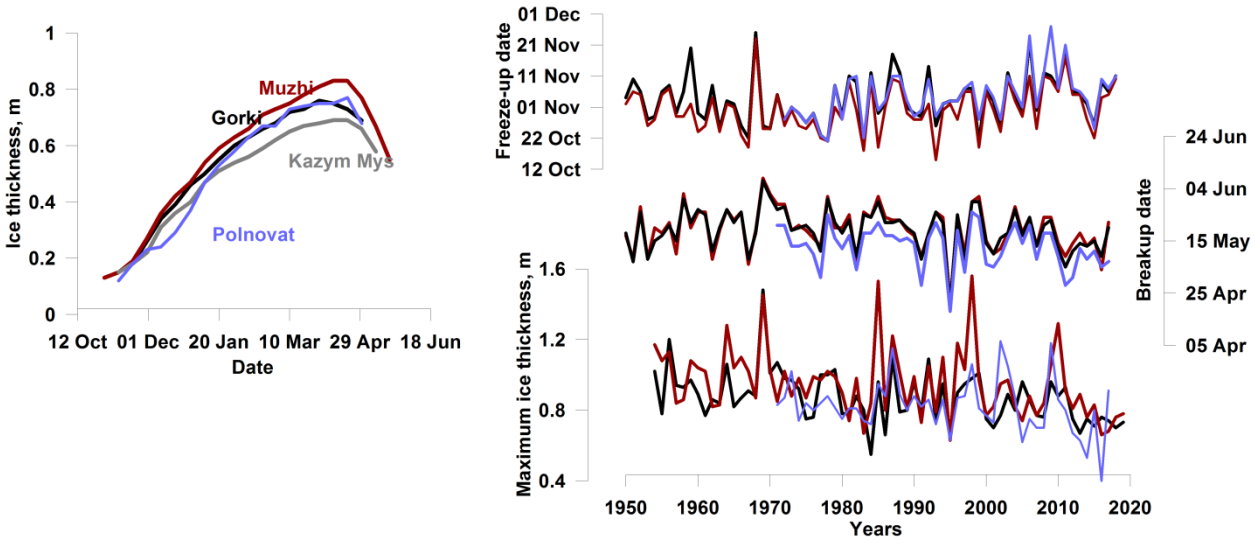

Figure 2. Examples of a) seasonal evolution of ice thickness (1980-2017 mean) at four stations (Gorki, Muzhi, Polnovat, and Kazym Mys) and b) interannual variability of ice freeze-up and end of breakup dates, and maximum ice thickness at Gorki, Muzhi and Polnovat stations.

3.2 Altimetry data

Data from the Jason-2 and Jason-3 satellite missions covering the period from July 2008 to August 2019 were used in this study. The Jason-2 satellite is the third altimetric satellite of the Topex/Poseidon-Jason series. The satellite operated between 2008-2016 and acquired data in a 10-day repeat orbit with an inclination of 66.08°. One satellite cycle consisted of 127 revolutions and 254 tracks (odd numbers for ascending and even numbers for descending orbits). The altimetric radar onboard Jason-2 provided along-track measurements at Ku (13.6 GHz) and C (5.3 GHz) bands with a sampling frequency of 20 Hz, allowing for a 375 m distance between adjacent radar measurements. The ground track repeatability of the mission was maintained within a ±1 km cross-track at the equator. At the latitudes of our study area (63-66°N), the cross-track oscillation band was approximately 400 m wide. Because the radar ground footprint at Ku-band is smaller than that at C-band, only measurements obtained at Ku-band were considered. The theoretical footprint of the radar at Ku-band is 10-12 km in diameter over a rough ocean surface. However, this diameter decreases over smooth inland water and ice surfaces such that the main returned signal can come from footprints of just a few kilometres in diameter (Legrésy and Rémy, 1997).

The satellite payload of Jason-2 also included a nadir-looking Advanced Microwave Radiometer (AMR), which provided measurements of brightness temperature at 18.7, 23.8, and 34.0 GHz frequencies with a sampling frequency of 1 Hz. Brightness temperature measurements acquired by other passive microwave radiometers, such as SSM/I and AMSR-E, have shown good performance for the retrieval dates associated with ice phenology (Kouraev et al., 2007; Kang et al., 2012; Du et al., 2017) as well as ice thickness (Kang et al., 2014) on large lakes in Russia and Canada. Since Jason AMR footprints are large in diameter (42 km at 18.7 GHz, 35 km at 23.8 GHz, and 22 km at 34.0 GHz) (Kouraev et al., 2007), the brightness temperature measurements over rivers are dominated by signals emitted mainly from land surfaces surrounding the river channels. Hence, we used Jason-2/3 AMR measurements only as a source of auxiliary information to develop additional criteria for adjustment of the radar freeze-up/breakup date retrieval algorithm. In 2016, Jason-3 was sent into space with the same orbit and instruments as Jason-2. For 20 cycles, the two missions flew with an 80-second time lag, ensuring continuity of measurements. During this period,

the difference in Ku-band backscatter (Sig0) between Jason-2 and Jason-3 was within 1 dB. The difference in the brightness temperature measurements was within 3 °K.

In this study, radar and brightness temperature measurements were extracted from a geophysical research data records product (GDR) distributed on the AVISO+ data portal (ftp-access.aviso.altimetry.fr, last accessed 30/06/2021). The GDR product contains various parameters estimated from the radar return echo, which is represented as a waveform. We used the 20 Hz backscatter coefficient retrieved from the ICE1 algorithm (Bamber, 1994). An altimeter waveform represents a histogram of energy backscattered by the ground surface to the satellite with respect to time. The waveform ground-processing consists in its retracking aimed at obtaining better range (distance from satellite to the Earth surface) estimates than those obtained with on-board algorithms. The ICE1 retracking algorithm calculates the centre of gravity, amplitude, and width of a rectangular box using the maximum power of the waveform samples. The backscatter is estimated using an instrument link budget and the waveform amplitude (ESA, 2020). AMR measurements of brightness temperature have a 1 Hz temporal frequency. Here they were linearly interpolated to the coordinates of the 20 Hz radar measurements.

Landsat 8 images at a 30-m spatial resolution (https://earthexplorer.usgs.gov/) were used for the geographical selection of altimetric radar and radiometer measurements over river channels using our own Python code allowing us to overlap along-track Jason-2/3 measurements on Landsat images. The cross-section of an altimetric track with a river channel is called a virtual station (VS; see Figure 1 for locations). Each VS was given a name containing the track number. To distinguish VSs located on secondary branches from those located on the main Ob River channel, the names of the stations located on the secondary branch (i.e. Small Ob River) were provided with the index "S_Ob".

4 Temporal variability of radar altimetry signal over frozen rivers

Since there is an absence of work on the use of radar altimetry for river ice studies, we provide some elements of interpretation on the evolution of backscatter with freshwater ice properties. The effect of varied ice properties on the radar return from nadir-looking altimeter instruments has been reported in several investigations of the Antarctic and Greenland ice sheets (e.g. Rémy et al., 2012; Nilsson, 2015; Larue et al., 2021) as well as for sea ice (e.g. Kurtz et al., 2014; Guerreiro et al., 2016). However, freshwater ice differs from other types of ice either by its textural/structural (e.g. crystal structure, density, layering, air bubble content) or chemical properties (e.g. salt content). The impact of freshwater ice properties on satellite measurements in the microwave region has been studied extensively in context of the interpretation of measurements from side-looking imaging SAR sensors (e.g. Duguay et al., 2002; Jeffries et al., 2005; Unterschultz et al., 2009; Atwood et al., 2015, van der Sanden et al., 2021). To date, no research has provided some explanations on the temporal variability of radar altimetry measurements over frozen rivers. Below, we provide a summary of the variability of altimetric radar signals over river ice during the freeze-up (ice formation), ice growth, and breakup (ice decay) periods.

Previous studies (e.g. Kouraev et al., 2005; Duguay et al., 2018; Zakharova et al., 2019, 2020) show that over Arctic rivers and lakes, that backscatter from radar altimeters varies seasonally. This behaviour is strongly related to hydrological phases, especially to the presence of ice (Figure 3a). We analysed the seasonal behaviour of backscatter from the Ob River with respect to geophysical parameters that can potentially affect the scattering properties of the surface at microwave frequencies. The radar return of nadir-looking altimeters significantly differs from the return obtained with side-looking imaging SAR instruments (ca. 20-45 degrees off nadir). At nadir, a smooth surface produces a higher return echo than a rough surface (Ulaby et al.,1986). The altimetric return signal is represented as

a waveform (Figure 3b). The shape of the waveform varies for different types of surfaces and can provide a variety of information useful for the interpretation of geophysical processes (Berry et al., 2005). For instance, Beckers et al. (2017) found the presence of an intermediate peak on the leading edge of waveforms that they attributed to reflection of the radar signal at the ice surface (i.e. snow-ice interface). The main waveform peak was considered to originate from the ice bottom (i.e. ice-water interface). The difference in ice surface - ice bottom altimetric heights estimated from these two peaks was found to be related to ice thickness and, therefore, used for its retrieval. In many of the radar waveforms extracted over river ice, we can also detect this intermediate peak on the waveform leading edge (Figure 3b). However, considering that the radar echoes over rivers come from very heterogeneous surfaces, we avoid referring to this peak to any definitive reflecting boundary and suggest another approach for ice thickness retrievals. Figure 3b demonstrates that during ice growth, the main waveform evolution is related to a decrease in power of the waveform main peak. This can be explained by the volumetric scattering/absorption of the radar signal with ice growth. We note that this decrease is proportional to the value of backscatter, which can be seen as the integral under the waveform. Based on this observation, we suggest that the retrieval of ice thickness is possible through the establishment of a simple statistical relation between radar backscatter and in-situ river ice thickness measurements. This simple approach has shown some potential for the retrieval of river ice thickness from imaging SAR instruments (Unterschultz et al., 2009; Mermoz et al., 2014). However, in contrast to nadir-looking radar altimeters, it has recently been suggested that backscatter from off-nadir looking imaging SAR during the ice growth season may be more related to increase roughness at the ice-water interface than ice thickness alone (Murfitt and Duguay, 2021).

High backscatter values of nadir-looking altimeters are observed when the instrument footprint contains a large fraction of open calm water (Fu and Cazenave, 1991). On rivers, over large, flooded areas, the water surface exhibits a certain roughness owing to turbulent flow and the impact of wind, thus resulting in lower backscatter values compared to calm water. On lakes, during freeze-up, the presence of floating ice (floes or slush) prevents the development of wind-induced waves and, therefore, increases the specular reflection off water (Kouraev et al., 2007). Freeze-up on rivers starts with the formation of a fine skim ice layer along the banks (i.e. border ice). This ice can detach and drift (Hicks, 2009). The skim ice is characterised by a smooth surface and smooth bottom. We suggest that the peak on the backscatter time series, at the time of appearance of the first skim or drifting ice in late autumn, can indicate the start of freezing (Figure 3c).

The scattering and absorption of radar echoes within ice depends on the penetration depth of the incident radar signal and internal ice properties (Rémy et al., 2012, Jeffries et al., 2012). At Ku-band, the penetration depth into dry freshwater ice is in the order of 5-12 m and depends on temperature and properties of the ice (Legrésy and Rémy, 1997). Therefore, in the case of thin lake or river ice, the penetration depth for waves emitted at altimetric radar frequencies (C and Ku-band) allows for the estimation of ice thickness. River ice mainly grows as water at the bottom of the ice cover freezes (Duguay et al., 2015). As ice grows, volume scattering of the radar altimeter signal within the ice increases resulting in a decrease in backscatter (Brown 1977; Rémy et al., 2012). On the Ob River backscatter time series, a distinct recession limb can be clearly observed in winter (see the red lines in Figure 3a). The Ob River ice gains approximately 30% of its total thickness during the first month of ice growth (Figure 2a). The highest temporal decrease in backscatter (Sig0), expressed as $\Delta Sig0/\Delta t$ (where Δt is the time-period between two consecutive observations), are observed exactly during that period. During winter, small peaks can appear in backscatter time series (see VS12 in Figure 3a). The peaks can be explained by temporary changes of ice surface characteristics such as the formation of polynya (open water areas), redistribution of snow on the ice surface by winds, snow wetting during mechanical ice cracking (i.e. slushing) as well as occasional snow melt during warm

sunny days (and refreezing at night) in early spring. All these processes either change the roughness of the reflecting surface (polynya, snow crust) or decrease the radar penetration depth and, consequently, reduce the signal energy loss within the ice.

River ice breakup is influenced by both thermodynamic and hydrodynamic processes, known as thermal and mechanical breakup, respectively (Ginzburg, 1977). Our previous studies using SARAL/AltiKa (Kouraev et al., 2015) and Jason-3 (Kouraev et al., 2021) altimeter data demonstrate that in early spring, when air temperatures are still mostly negative, lake ice undergoes metamorphism under the influence of solar radiation. At that time, a drop in backscatter in the order of 5-10 dB can be observed. A similar process can occur on the Ob River ice during the pre-melt period (see, for example, years 2012-2016 in Figure 3a). When air temperatures become positive, snow on the ice surface melts, increasing the surface backscattering of the radar signal. Melt progressively affects the ice and melt ponds with a smooth water surface can appear on the ice surface. The presence of water on the ice surface and wet snow/ice prevents the penetration of radar signals (Ulaby et al., 1986). During melt, surface scattering becomes dominant in altimetric return signals. This leads to an increase of radar altimetry backscatter as the roughness of the surface of the melting snow/ice and melt ponds is low.

Mechanical breakup begins when the water level rises. At this time, water can flood the ice surface due to earlier breakup in the river headwaters or its tributaries, or due to water infiltration through cracks in the weakened/fractured ice (Ginzburg, 1977; Hicks, 2009). A high backscatter peak occurs at the beginning of flooding. The value of the peak varies over a large range, in the order of 25-50 dB. Such events preclude the development of a threshold-based algorithm for the retrieval of breakup dates. As the river becomes ice-free, the backscatter decreases owing to the increased surface roughness induced by wind and turbulence.

During the open water season, several backscatter peaks are frequently observed. Summer variability in backscatter depends on many factors, including, but not limited to, wind induced roughness, VS location (banks, presence of islands, floodplain characteristics), and the proportion of water within the footprint (intermittent summer inundation due to rain events).

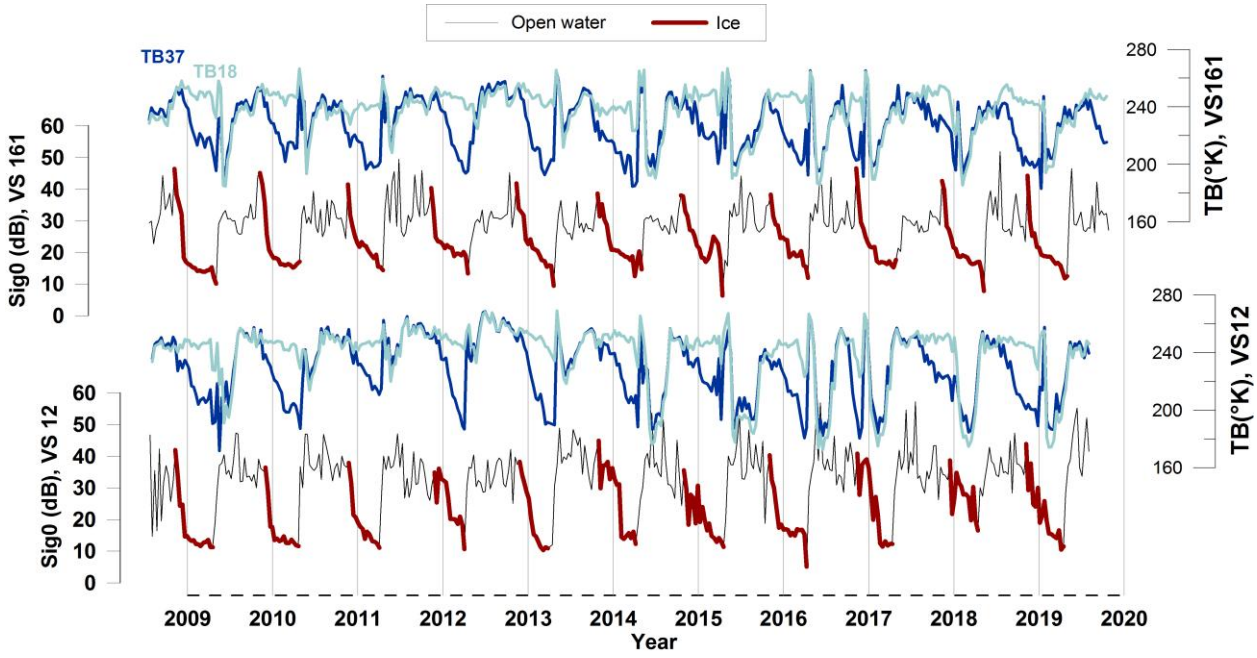

a)

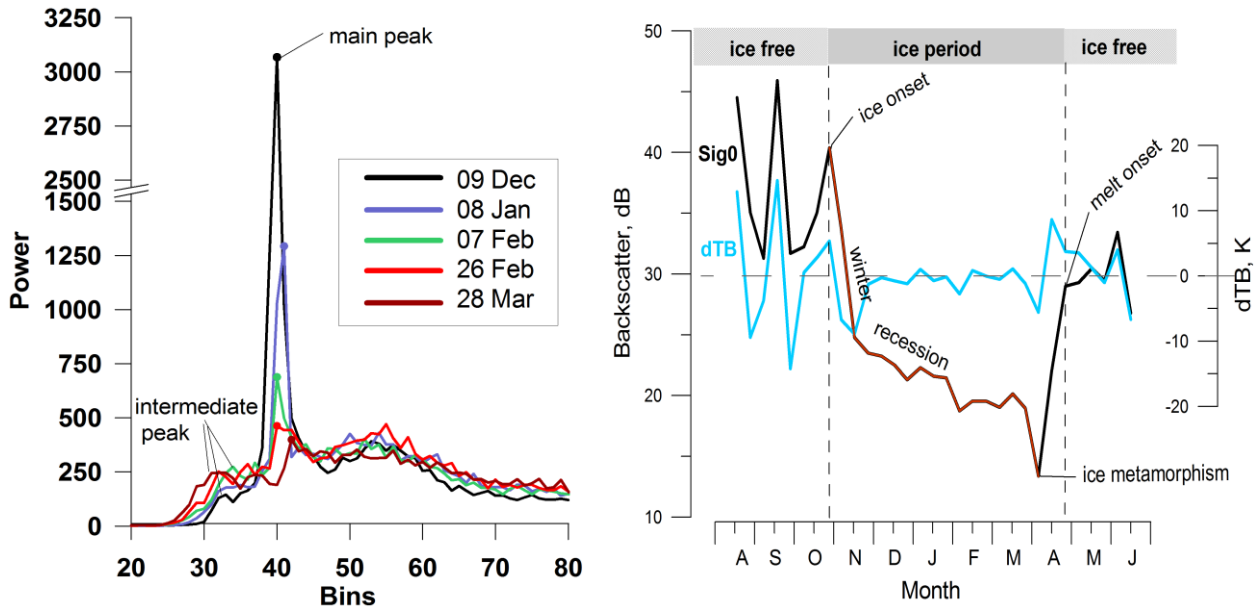

Figure 3. Variability of Jason-2/3 measurements over sections of the Ob River. a) Interannual variability of backscatter and brightness temperature to the north (VS 161) and south (VS 12) of the study area (dark red lines correspond to the ice cover period retrieved from altimetric measurements). b) Winter evolution of typical waveforms for track 88 over a river channel (the coloured lines correspond to different dates during winter 2013-2014). c) Typical seasonal variability of backscatter on the Ob River and related ice regime phases.

5 Methods

5.1 Ice onset and breakup algorithm

Considering the behaviour of radar backscatter over frozen rivers described in Section 4, we developed a dynamic algorithm for retrieving ice phenology dates based on the analysis of Sig0 time series specific to each VS. We suggest that the last annual peak of each year in the backscatter time series corresponds to the beginning of river ice formation (ice onset). In the case of a multi-peaky recession limb, see for example VS12 in 2013 (Figure 3a), we select the peak height of the order of spring-summer peak heights typical for this VS. If the selection of the peak is not straightforward (for example, two high peaks within one month or the prominence of the peak is low), an additional criterion based on the brightness temperature difference between the 34.0 and 18.7 GHz frequency channels (ΔTB) is introduced. In such case, we select the backscatter peak at time *t*, if in a time frame of (*t*-1, *t*+2) of satellite cycles at least three of the four ΔTB values are <2° K.

$$N_{MS} = length\left(max\left(Sig0_{Oct-Dec}\right)\right), \quad N_{dTB} = length\left(\Delta TB_{t-1:t+2} < 2\right)$$

where N_{MS} - number of detected peaks, N_{dTB} - number of ΔTB observation.

$$\begin{cases} N_{MS} = 1, & \rightarrow \quad ice\ freeze-up\ date \\ N_{MS} > 1, \quad N_{\Delta TB} \geq 3, & \rightarrow \quad ice\ freeze-up\ date \end{cases} \tag{1}$$

Brightness temperature measurements integrate emissions from larger surrounding areas than the altimetric radar backscatter measurements. Freezing of small oxbow lakes on the floodplain as well as soils and bogs on banks usually occurs earlier than in the big channels of the Ob River. By applying the (t-1, t+2) window, we ensure that

the progression of freezing in the area of the VS is captured and that the backscatter peak is not caused by a synoptic-scale cooling episode or by calm weather conditions.

The beginning of the ice cover decay (thermal ice melt start) leads to an increase in spring backscatter. The melt-detection algorithm searches for the spring peak in the backscatter time series. For multi-peak winters, the algorithm also uses the ΔTB condition. In this case, the algorithm searches for the peak which is accompanied by a simultaneous increase in ΔTB in the same order of magnitude as the mean summer ΔTB value for a given VS. In a few instances, the spring peak is found to be absent or cannot be automatically detected because of a low prominence. In these cases, we use the date of maximum increase in backscatter between two satellite cycles (ΔSig0/Δt) for the period from January to mid-June.

$$N_{MS} = length\left(max\left(Sig0_{Apr-Jun}\right)\right), \quad S\Delta TB = mean\left(\Delta TB_{Jul-Aug}\right)$$

where N_{MS} - number of detected peaks, $SdTB$ - mean summer dTB for a given VS.

$$\begin{cases} N_{MS} = 1, & \rightarrow \quad breakup\ date \\ N_{MS} > 1, \quad min(\Delta TB_t - S\Delta TB), & \rightarrow \quad breakup\ date \\ N_{MS} = 0, \quad max\left(\Delta Sig/\Delta t_{Jan-Jun}\right), & \rightarrow \quad breakup\ date \end{cases} \tag{2}$$

A variety of combinations of different geomorphological (riverbanks, floodplain, river width, islands), meteorological (synoptic cooling/warming episodes), and ice cover/open water (polynya, ridging) conditions can occur. Their complex impact on the variability in backscatter during freeze-up and breakup makes it difficult to address all variations in an automated manner. Because of this, we retrieved the ice phenology dates manually through visual inspection of backscatter (and ΔTB if necessary) time series for each VS as to compare the performance of the automated and manual freeze/melt detection routines. Both, manual and automated routines use the same criteria. A summary of the processing scheme is illustrated in Figure 4.

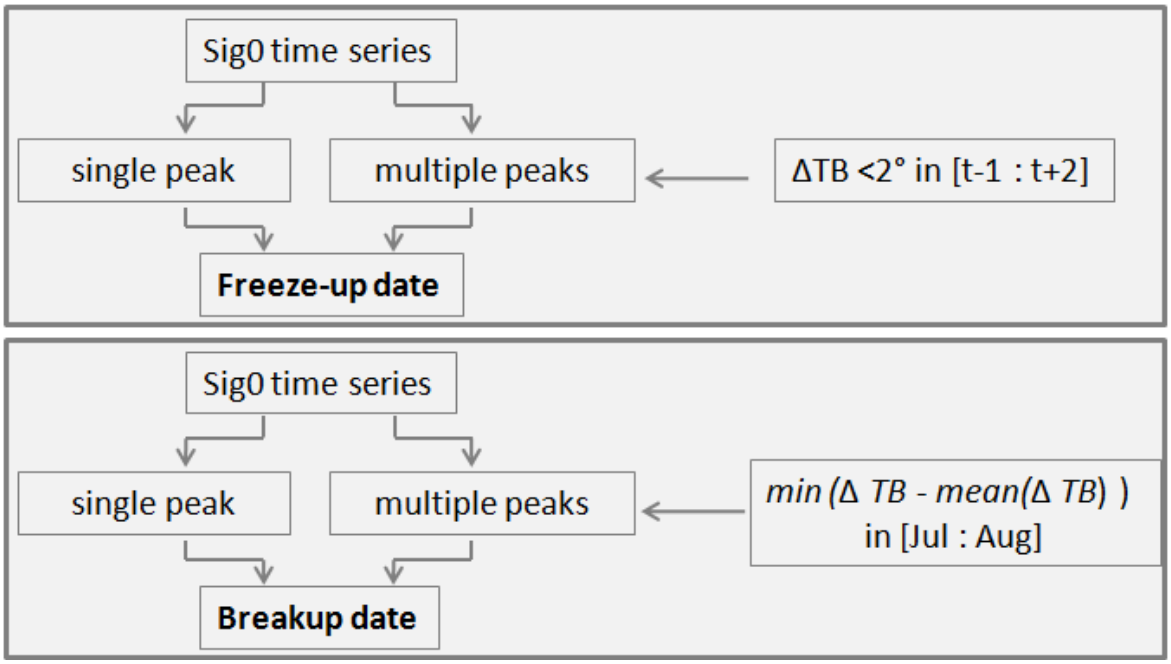

Figure 4. Processing scheme of ice phenology dates retrieving from altimetric measurements.

5.2 Ice thickness algorithm

Year-to-year variations in the backscatter values at the beginning of the freeze-up period (see Figure 3a) may be caused by different land/water/ice proportions within the radar altimeter footprint, wind conditions, floating ice concentration, etc. Assuming that the decrease in backscatter between two consecutive observations ($\Delta Sig0/\Delta t$) is proportional to a gain in ice thickness (see Section 4), we use a relative backscatter decrease rather than the absolute backscatter values for the estimation of ice thickness. This allows us to minimise the effect of the initial freezing conditions on the accuracy of ice thickness retrievals. Starting from the first date of freezing (i.e. ice onset determined manually), we estimate the backscatter cumulative difference $\Sigma(\Delta Sig0/\Delta t)$ and construct the relationship between this parameter and in-situ ice thickness (Hice) measured at the nearest gauging station (Figure 5). The application of a Locally Estimated Scatterplot Smoothing filter (LOESS) on the $\Sigma(\Delta Sig0/\Delta t)$ parameter makes it possible to minimise the effect of secondary peaks on the backscatter winter curve.

Along the 400 km long Low Ob River reaches covered by the 20 northernmost Jason satellite tracks, 48 VSs were defined using Jason-2 and 3 tracks overlayed on Landsat 8 images. 10 VSs nearest to the five gauging stations were chosen as a training set for calibration of the ice thickness retrieval algorithms and for estimation of uncertainties in ice phenology dates and ice thickness retrievals. Results of the retrievals of ice onset and ice melt start dates by both the automated and manual routines were compared to the ground station records of ice types or water/ice cover state (ridging, polynya, water-on-ice, ice drift, etc.). As the dates of in-situ measurements do not coincide exactly with the Jason overpass dates, ice thickness values were linearly interpolated between two adjacent dates of in-situ observations for the dates of satellite overpasses. The other 38 VSs (main set) were used to characterise the ice conditions within all studied river reaches.

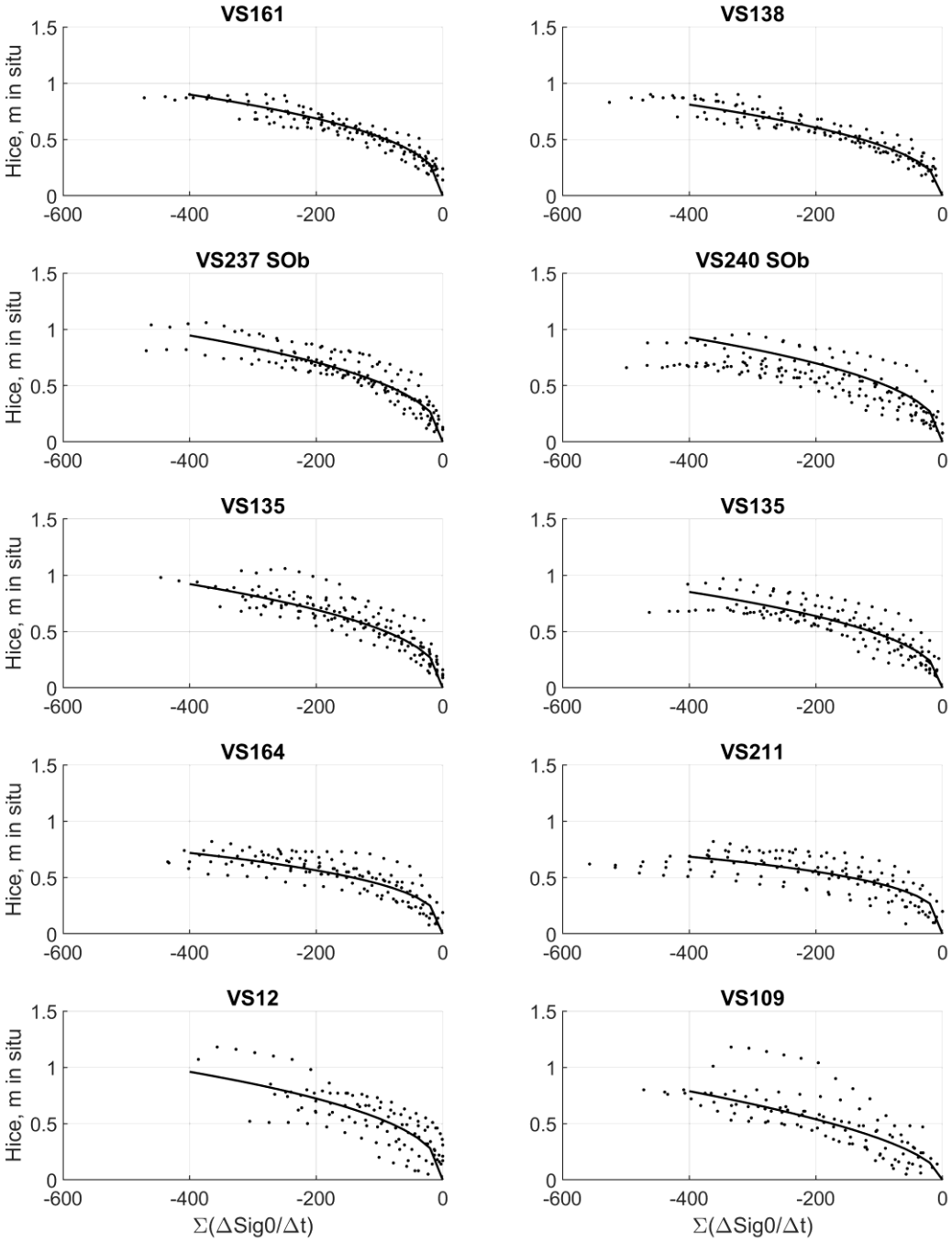

Figure 5. Relation between Σ(ΔSig0/Δt) and in-situ ice thickness at ten virtual stations.

Amongst the tested fitting functions (linear, polynomial and power), the power equation (3) produced the best fit between the cumulative backscatter difference and in-situ ice thickness measurements. The selection of the fitting function was based on maximisation of correlation between Σ(ΔSig0/Δ*t*) and in-situ Hice and minimisation of root mean square error (RMSE) calculated between retrieved from equation 3 and observed Hice.

$$Hice = a \times abs(\Sigma(\Delta Sig0/\Delta t))^{b} \quad (3)$$

Coefficients a and b of the equation were estimated for each pair of gauging - VSs from the training set. Using the leave-one-year-out method (Picard and Cook, 1984) for each VS - gauge station pair, we obtained a set of a and b coefficients and estimated their mean values. These mean values were then used for ice thickness estimation on the corresponding training VS. The accuracy of the ice thickness retrievals was evaluated using the correlation coefficient and RMSE calculated between retrieved and observed ice thickness for the 2008-2018 period. A schematic representation of the processing steps is presented in Figure 6.

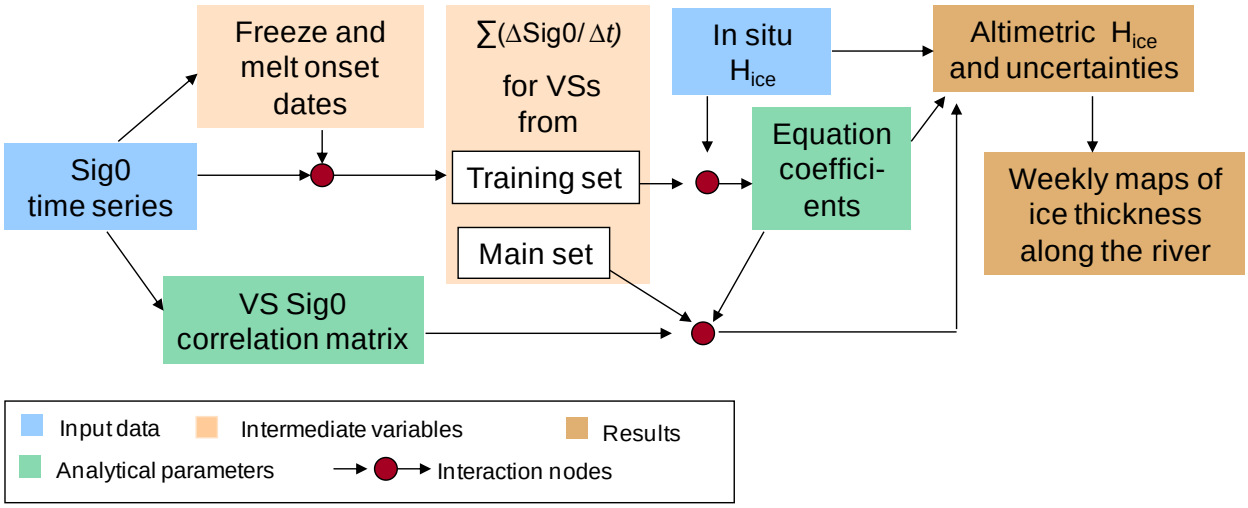

Figure 6. Processing scheme of ice thickness retrieving from altimetric measurements.

5.3 Generation of 2D spatio-temporal ice thickness product

Using coefficients a and b from equation (3) derived for the VSs from the training set, we estimated the ice thickness at locations of the other 38 VSs. The following strategy was adopted: firstly, for each VS, using the correlation matrix, we searched for the best correlation between its backscatter and the backscatter at one of the training VS_t. Then, the coefficients a and b of VS_t showing the highest correlation coefficient were applied to the VS considered.

Ice thickness retrieved at all 48 VSs were used for the creation of weekly maps, which were generalised into a 2D spatio-temporal ice thickness product. For this, the altimeter-derived ice thicknesses were interpolated and smoothed in 2D spatio-temporal coordinates using a moving average filter. The size of the smoothing window must: a) preserve as much as possible the Hice magnitudes and the spatial heterogeneity of ice thickness in the spatial domain; and b) reduce the residual noise in the temporal domain remaining after smoothing of the backscatter time series with the LOESS filter. The selection of the smoothing window was determined based on the correlation coefficient and RMSE estimated between Hice time series retrieved at virtual stations and Hice time series extracted from the smoothed product for the same VS locations. The effect of interpolation and smoothing on seasonal Hice magnitude was evaluated via estimation of the difference between maximum yearly values of Hice.

It should be noted that an important effect of the interpolation/smoothing procedure on Hice (i.e. rapid degradation of the correlation coefficient and RMSE statistics) occurred in a 15-40 km spatial window range. In windows beyond 40-45 km, the procedure resulted in little subsequent changes in the smoothed product. In the temporal domain, the application of windows below 15 days (for 0 km spatial window) and 40 days (for 60 km spatial window) also had a minor effect (the correlation coefficient was above 0.98, RMSE and difference in maximum Hice ($Hice_{max}$) were below 0.03 m). The selected window of 40 km/30 days allowed to keep the average

$Hice_{max}$ difference and RMSE below 0.04 and 0.03 m, respectively. The correlation between Hice time series extracted from the smoothed product and those retrieved at 20 VSs located on the main branch of the Ob River was 0.99.

5.4 Validation of ice phenology retrieval algorithm

Considering the 10-day repeat overpass of the Jason-2/3 satellites and the distance between the gauging stations and VSs, we considered a 10-day time-step difference (i.e. ±10 days) as an acceptable accuracy for altimetry-derived ice phenology dates. For 90% of the manual routine retrievals, the difference in the first ice events (ice onset) with in-situ observations is less than 10 days (Figure 7a). In 56% of the cases, there is no difference in the number of days. As the radar footprint over rivers is heterogeneous and is affected by signals from the frozen/unfrozen state of land/river/floodplain lakes, there are numerous variations in the behaviour of backscatter at the beginning of the freeze-up period. In such case, the automated routine misses certain behaviour types, and detection is less accurate for ice onset than in the case of the manual routine. Only 70% of the altimetric ice onset dates fall within 10 days of the in-situ observations at gauges, and only 40% fall on the same day.

Breakup is a more complex process consisting of the thermal degradation of ice cover (melt start) and its mechanical disintegration and downstream movement (melt end). Comparing the dates of altimetry-derived melt onset (start) with the ice state flags provided by gauging stations, we could conclude that the manual routine of our algorithm accurately detected the start of ice thermal degradation. In 88% of the cases, the difference between the manually retrieved melt dates and in-situ observations of the first water appearance is less than ±10 days (Figure 7b). The automatically derived melt date estimations are less accurate for the detection of melt starts compared to the manually derived estimations. However, the automated routine is more adapted for the detection of the melt end than for detection of melt start; an accuracy of less than ±10 days is achieved for 67% of cases (Figure 7 b, c).

The melt algorithm was designed for detection of the ice melt start, i.e. the wet ice, water-on-ice or open water events. Manual retrieval of breakup dates allows for better control over the complex variability of backscatter in spring than does the automated routine. It is likely that in the complex cases the automated routine detects the melt end or even provides unrealistic early/late estimates of melt dates. For example, for the whole set of 48 VSs, over the full 10 winter periods of study, the automated detection fails, that is detects unrealistic melting dates before 10 April and after 10 June, in 10% of the cases. As the manual routine demonstrates better accuracy than the automated one, it was therefore selected for further analysis of results and for use with the ice thickness retrieval algorithm.

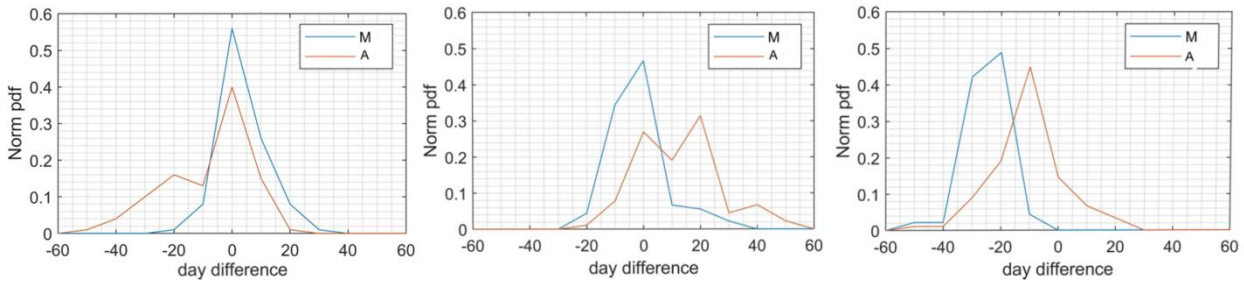

Figure 7. Normalised distribution of difference in number of days between altimetric and in-situ observed dates of a) ice onset, b) melt start, and c) melt end over 2008-2019 period for 10 virtual stations from training set of VSs. Legend: M - manual routine; A - automated routine.

A comparison of the interannual variability of median dates estimated for VSs located on the main river branch (20 VSs in total) with the corresponding parameter estimated from observations at four gauging stations (also located on the main river branch) demonstrates a good agreement between satellite retrievals and in-situ observations (Figure 8). A significant difference between gauging and VSs (in the order of 20 days) is observed only for melt start dates in 2014. This good agreement suggests that our algorithm is suitable for monitoring the interannual variability of ice events.

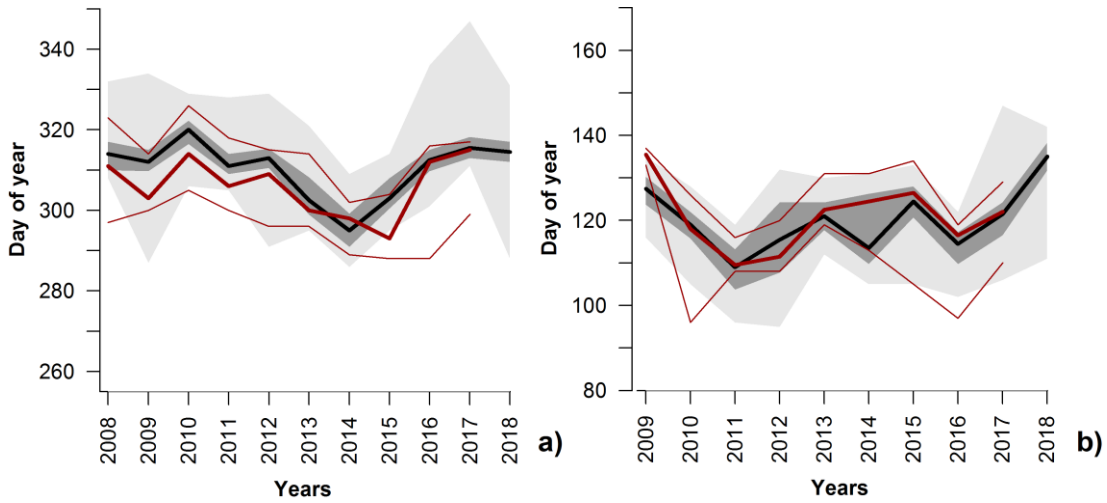

Figure 8. Interannual variability of dates of a) ice onset and b) melt start for the main Ob River channel retrieved using the manual routine. Red thick lines are the median and red thin lines are the min-max values observed at four gauging stations along the main Ob River channel. Black thick lines correspond to the median value of dates observed at 20 virtual stations within the same river reaches. The dark grey zone is the spread between the 3rd and 1st quartiles, and light grey zone is the spread between minimum and maximum values.

5.5 Validation of ice thickness retrieval algorithm

The accuracy of ice thickness retrievals from altimetric measurements was assessed for the ten VSs from the training set located around the gauging stations (Figure 9). At the northern VSs (VSs 161, 138, 237S_Ob, and 249S_Ob), the correlation between retrieved and observed ice thickness is stronger than at other locations, and the RMSE in estimates of the altimeter-retrieved ice thickness are less than 0.12 m (Table 2). For the southernmost VSs (VS 12 and 109), the RMSE increases up to 0.14-0.18 m. The relative uncertainty in ice thickness estimates is found to be higher at the beginning (low Hice) of the ice period, compared to the Hice retrievals in the middle or end of winter. Except for VS109, the variability in the values of coefficients a and b in Equation (1) is low (Table 2), which indicates good stability in the established relationships and their potential validity for other VSs located far from the gauged reaches. One way to evaluate the sensitivity of the satellite Hice retrievals to fitting parameters consists of running a cross-validation experiment, i.e. retrieving the Hice using the coefficients obtained for an adjacent VS. Similar scores between retrieved and in-situ ice thickness obtained in validation (Table 2) and in cross-validation (Table 3) experiments demonstrate the robustness of equation 3, resulting in low errors in satellite Hice estimates for the northern VSs (161, 138, 237S_Ob, and 249S_Ob). Uncertainties of Hice retrievals for the southernmost VSs are higher than for the northern VSs. However, the retrievals at the southern VSs in the cross-validation experiment can

460 be improved by selecting the equation parameters (a and b) not from the adjacent VS, but from the training VSs, which provide the best Sig0 correlation with the Sig0 of VSs considered. For example, when applying the coefficient derived for VS135 - Gorki gauging station pair to VS109 and VS12 (backscatter of the VS135 demonstrated the highest correlation with the backscatter of the VS109 and VS12), the RMSE of retrieved Hice for these VSs decreases from 0.23 m to 0.18-0.19 m (see scores in the denominator of corresponding lines in Table 3).

465

Table 2. Coefficients a and b for built relations, correlation coefficient (R) and RMSE between retrieved and in-situ ice thickness for virtual stations from training set. S_Ob refers to virtual stations located on the secondary (western) river branch of the Ob (see Figure 1).

Virtual stations	Corresponding gauging station	Distance to gauging station, km	Coefficients of equation (3)		Validation scores	
			a	b	R	RMSE, (m)
161	Pitlar	5.6	8.69	0.39	0.94	0.07
138	Pitlar	5.1	6.54	0.42	0.94	0.07
237 S_Ob	Muzhi	15.9	7.64	0.42	0.90	0.10
240 S_Ob	Muzhi	7.7	7.96	0.41	0.90	0.10
240	Gorki	19.4	7.70	0.39	0.81	0.12
135	Gorki	28	6.88	0.42	0.87	0.11
164	Kazym Mys	22.4	8.83	0.35	0.84	0.10
211	Kazym Mys	20.1	10.7	0.31	0.76	0.12
12	Polnovat	10.9	8.23	0.41	0.77	0.18
109	Polnovat	33.4	2.92	0.55	0.84	0.14

470

Table 3. Correlation coefficient (R) and RMSE between retrieved and in-situ ice thickness in cross-validation experiment.

Virtual stations	Corresponding gauging station	VS whose coefficients a and b are used for cross-validation	R	RMSE (m)
161	Pitlar	138	0.94	0.09
138	Pitlar	161	0.94	0.09
237 S_Ob	Muzhi	240 S_Ob	0.90	0.10
240 S_Ob	Muzhi	237 S_Ob	0.89	0.11
240	Gorki	135	0.81	0.13
135	Gorki	240	0.87	0.11
164	Kazym Mys	211	0.84	0.10
211	Kazym Mys	164	0.76	0.13
12	Polnovat	109/135*	0.76/0.76*	0.23/0.18*
109	Polnovat	12/135*	0.76/0.76*	0.23/0.19*

* Two different pairs of a and b coefficients were used for cross-validation.

475

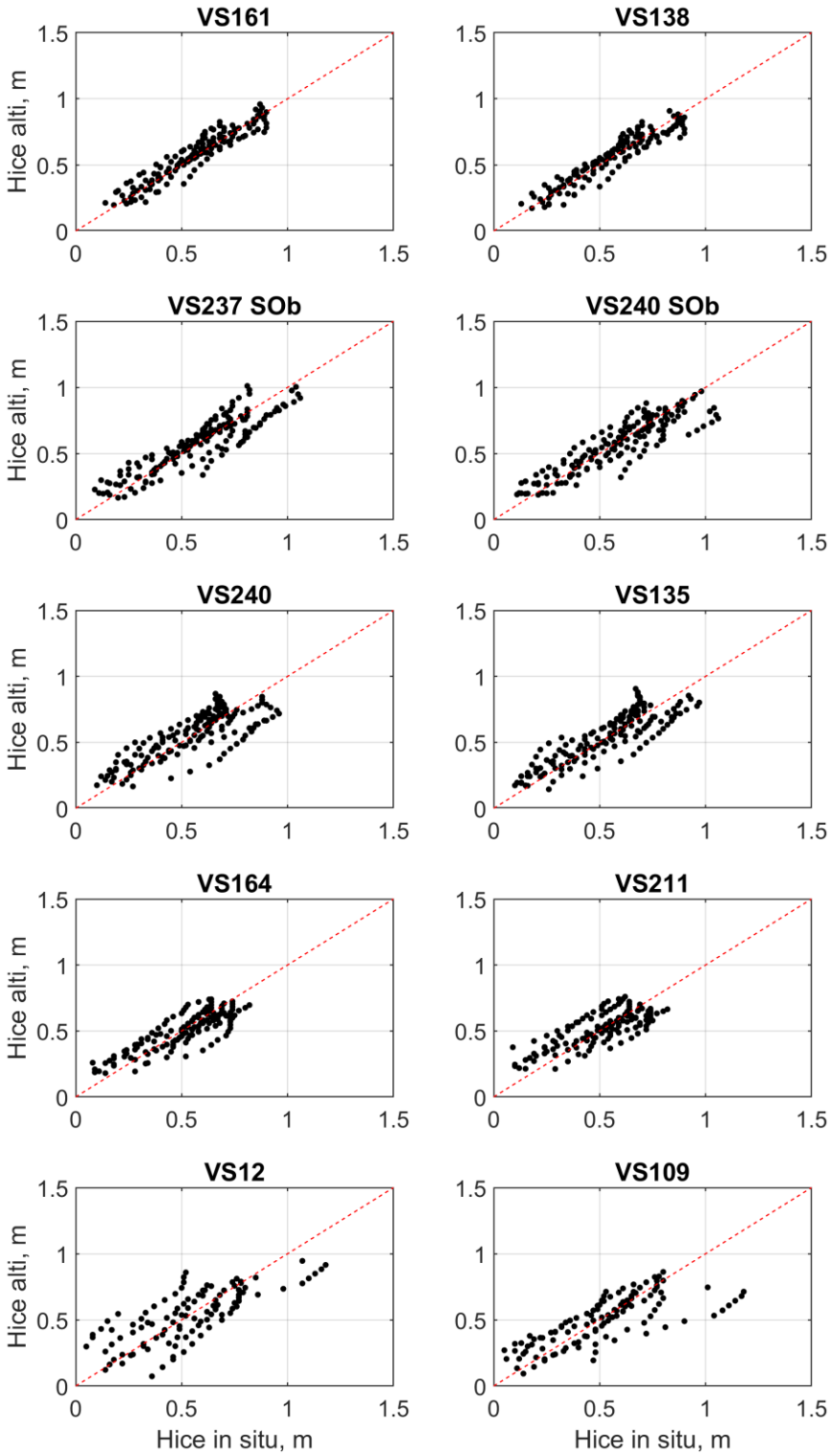

Figure 9. Ice thickness measured at gauging stations (x axis) and retrieved from the altimetric measurements (y axis) for training VSs. The red dash line corresponds to the 1:1 relation line.

6 Results

6.1 Ice thickness estimation for the entire studied river reaches

Using the a and b coefficients of Equation (3) developed for the VSs from the training set, we estimated the ice thickness at locations of the other 38 VSs and produced weekly maps, which were generalised into a 2D spatio-temporal ice thickness product (Figure 10). The elaborated maps can be used for evaluation of ice thickness and ice phenology dates in areas between virtual stations. For instance, two useful parameters can be extracted from the 2D product: the maximum ice thickness and ice thickness observed on 1 December.

From a practical standpoint, knowledge of the maximum ice thickness is relevant for hydro-climate change monitoring (Vuglinsky and Valatin, 2018), while the ice thickness determined on 1 December is crucial for local and regional socioeconomic stakeholders as this is the average date for the opening of the ice bridge road to the north of the study area at Salekhard. To assess the quality of the 2D product for operational use, we compared the interannual dynamics of the mentioned parameters derived from this product and observed at the gauging stations.

For ~90% of the area of the studied river reaches, the interannual variability in maximum ice thickness retrieved from altimetric measurements indicates a clear decrease from 2008 to 2012 (Figure 10). This tendency corresponds well to those observed at all gauging stations (Figure 11a). Since 2013, the maximum ice thickness has increased slowly. However, altimetric and in-situ observations after 2013 both exhibit spatio-temporal variability that is not always in agreement. This disagreement may be related to environmental factors affecting ice growth, such as snow amount, autumn ice drift and accumulation, ridging/hummocking, and ice flooding (water-on-ice). For example, according to station records, ridging events appear more frequently after 2012 at the northernmost gauging station, Pitlar, than at other gauging stations. We cannot fully exclude the effect of the simplicity of the retrieval algorithm, based on the empirical approach, as well as the effect of spatio-temporal smoothing of the altimetric retrievals used in map production.

Differences between altimetric and in-situ ice thickness on 1 December lie within the algorithm uncertainties of 0.07-0.18 m (Figure 11b). In addition to the geophysical reasons and simplicity of the algorithm noted above, the observed difference can be related to degradation in the quality of the in-situ time series (gaps, unrealistic values) and the low representativeness of the one-hole sampling protocol for in-situ ice thickness measurements.

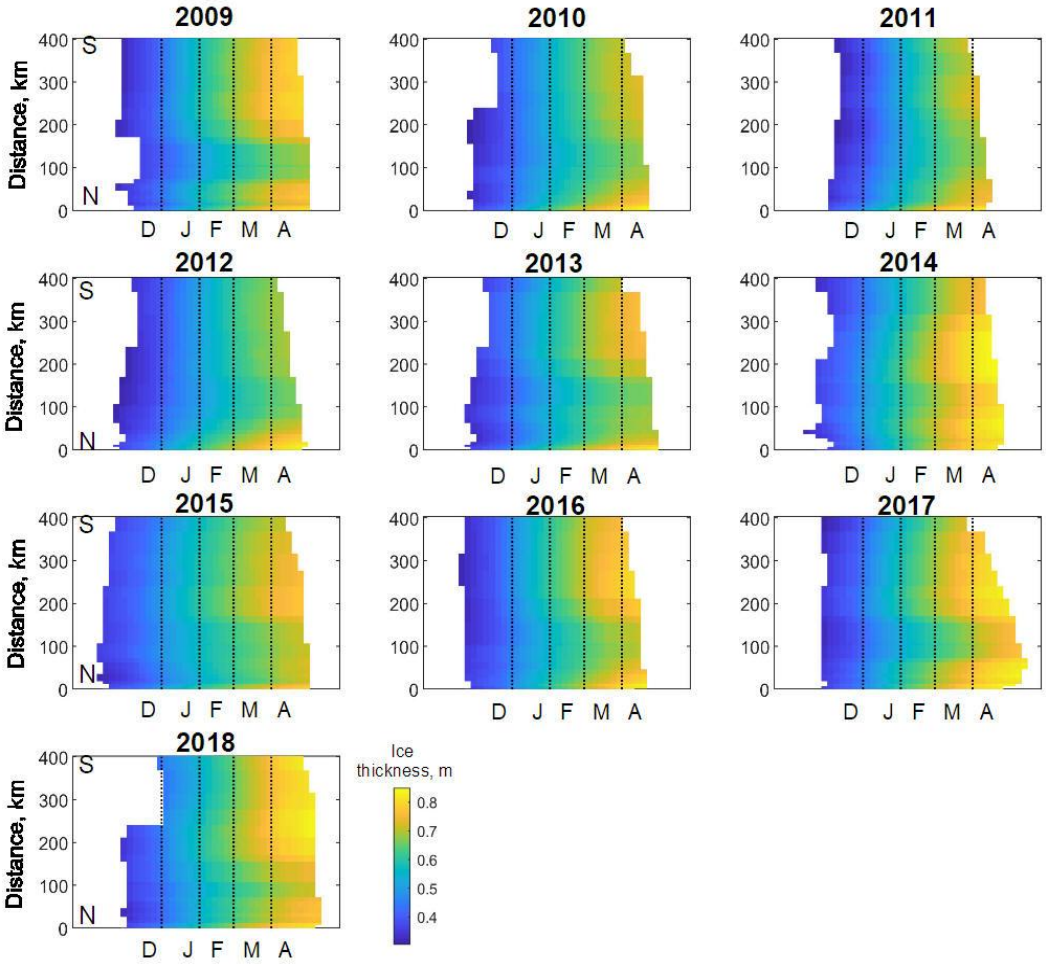

Figure 10. Spatio-temporal ice thickness variability (m) for the main branch of all Low Ob River reaches for the 2008-2018 period from generalized weekly altimetric product. Distance in km is indicated from the northernmost virtual station 187 in the upstream direction (south). Letters on the x axis correspond to the first letter of the month (December-April).

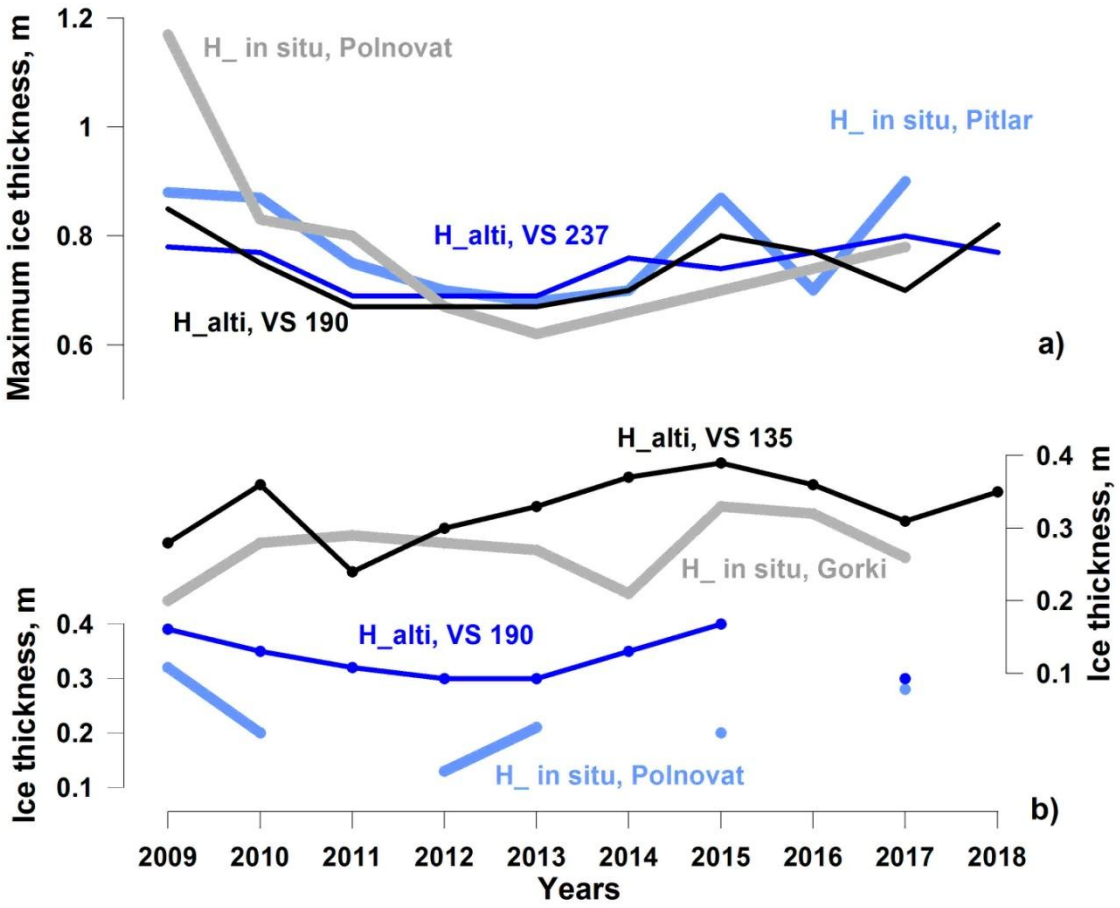

Figure 11. Interannual variability of ice thickness extracted from 2D ice thickness product at VS 237, 190 and 135, and observed at gauging stations: a) maximum ice thickness and b) ice thickness on 1 December.

6.2 Winter ice bridge roads operation forecast

In many regions with seasonal ice cover, frozen rivers enhance the interconnection and supply of many small, and even some large, cities. Many remote villages that are linked in summer to supply centres only via expensive aircraft or boat transport can directly access the main land transport arteries built on frozen-ground and lake/river ice. The importance of ice roads is highest for the Arctic regions where the construction of permanent bridges is restrained by the presence of permafrost and its destabilisation.

A good example is Salekhard City located on the Ob River near the polar circle in the zone of discontinuous permafrost. The city has 50 000 inhabitants and is supplied primarily via the Northern Railway, which connects the small town of Labytnangi on the left bank of the Ob River with the European part of Russia and the main supply centres. Merchandises from Labytnangi are delivered to Salekhard by ferry. Every winter, an ice road is constructed to ensure the transport of goods and people. Owing to security reasons, the ferry ceases operation after the appearance of the first ice. The ice road construction (artificial growing of ice thickness via pumping of water on the ice surface) begins when the ice thickness attains an allowed value of 0.20-0.25 m (Instructions on Safety Organisation, 1969). The traffic of light vehicles is allowed when the ice thickness exceeds 0.30 m. According to information kindly provided by the State Traffic Service of Yamalo-Nenetzky Autonomous District (Russia), the ice road operation usually starts 3-4 weeks after the beginning of freezing, with an average opening of 30 November – 1 December. The road operation closes gradually starting from the limitation of the lorry load in the middle of April

until full halt at the beginning of May. The ferry connection is restored approximately three weeks later. Between the ferry and the ice road operation, the connection is ensured via a hovercraft boat only for a limited number of passengers or for emergencies.

Dates of the autumnal halt of ferry operation for 2010-2018 agree very well with those of the first ice occurrence on four northernmost tracks of the Jason satellite located 65-75 km south of the city. For the short-term forecast, the satellite observations in the area of VSs 112 and 9 are especially good and allow for the prediction of the end of ferry operation four days in advance. We assume, further, that an average value of the dates when satellite derived Hice at the four northernmost VSs reaches 0.30 m may provide an estimate for the road opening date. These dates were extracted from the spatio-temporal smoothed maps and compared with the dates of ice roads opening provided by the State Traffic Service. The mean difference between satellite and observed dates was four days (Figure 11a). However, in half of the years, the predictions differ from observations by more than five days (11 days maximum). As noted in Section 6.1, at the beginning of freezing, errors in Hice retrievals are quite high, and ice thickness is often overestimated (see Fig 11b). Based on this fact, we consider that at present the altimetric algorithm and the ice thickness product are not sufficiently accurate for operational ice road opening forecast. Nevertheless, their accuracy is sufficient for the assessment of climate impacts as we capture the interannual variability of dates of ice road opening (Figure 12a).

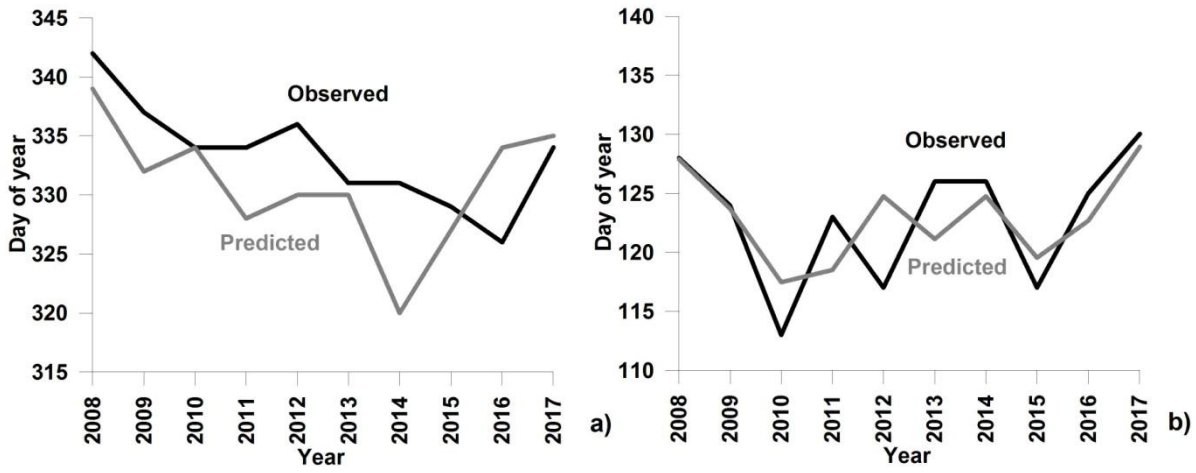

Figure 12. Observed and predicted from the altimetric satellite observations dates of Salekhard ice road a) opening and b) closing.

For the prediction of dates, when the ice road at Salekhard ceases its operation, the use of the northernmost VSs was not possible as traffic on the ice road closes before the altimeter detects the breakup onset on this reach. However, the satellite observations of breakup onset at VSs located in the upper reaches can provide the necessary information. Using altimetric retrievals of the breakup start for the entire set of 48 VSs, for each year, we searched the date when at least two altimetric breakup onsets (AMO2) were detected within the entire 400 km river reaches. This date served as a predictor of the date of ice-road closure at Salekhard. The correlation between AMO2 and observations is significant (p-value = 0.025) with a correlation coefficient of 0.70 (Figure 13a). After applying a correction to AMO2 computed from the relationship shown in Figure 13a, one can obtain a forecast date of ice road closing at Salekhard and evaluate the residual difference between forecasted and observed dates. This difference, expressed as RMSE, is three days (see Figure 12b). The leading time of the forecast can be determined from the plot shown in Figure 13b. It varies from four days (for late breakup start) to 22 days (for early breakup start).

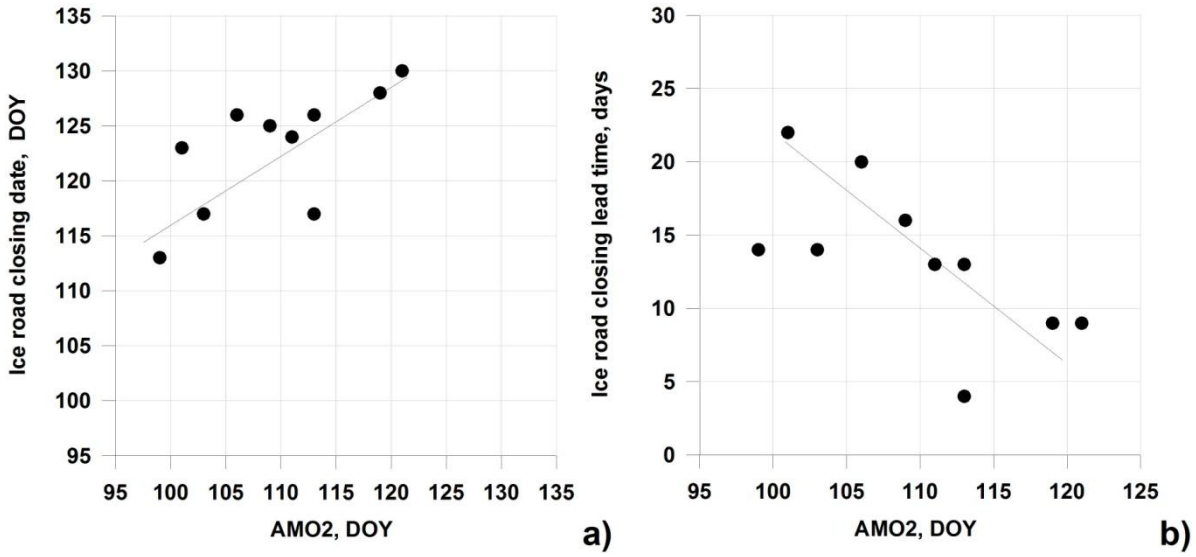

Figure 13. Relation between altimetric breakup onset dates (AMO2) and observed at Salekhard ice road closure dates expressed in days of year (DOY).

7 Discussion

7.1 Factors affecting ice thickness retrievals from altimetry

Various factors can affect radar return echoes and, consequently, the accuracy of river ice thickness retrievals. One source of uncertainty could originate from the underestimation of the role of snow-on-ice in microwave signal scattering (King et al., 2013, 2015). However, Willatt et al. (2011) showed that the Ku-band electromagnetic wave scattering by snow at nadir is low, and in our study, we neglected the presence of snow on ice. Using precipitation data from the nearest meteorological station, we noted that not all heavy snow accumulation episodes affected the backscatter over river ice. In several cases, snowfall resulted in backscatter changes in the order of 1.5 dB. The smoothing procedure applied to the cumulative $\Delta Sig0/\Delta t$ series helped to eliminate this effect. Moreover, after adding the in-situ snow depth to the ice thickness, we noted that the Hice - $\Sigma(\Delta Sig0/\Delta t)$ power relationship becomes weaker.

Another factor potentially affecting the backscatter value over freshwater ice is ice roughness at the ice-water interface (Atwood et al., 2015). The roughness of the ice bottom on the rivers is expected to be high at the beginning of the freeze-up period in bridging areas, where floes juxtapose and accumulate underside. Any rough boundary dissipates the signal of nadir-looking radar instruments, resulting in a decrease in backscatter. Further congelation of the inter-floes volume as well as ice growth both lead to levelling of the ice low boundary. We suggest that the under-ice current may also contribute to the ice bottom levelling at the Ku-band radar wavelength scales (~1-1.5 cm). This levelling would increase the radar return power during winter. However, we did not find evidence of this process in the backscatter time series (see Figure 3a). Either the levelling effect is weak and is masked by high volumetric scattering of the radar echo within thickening ice, or at the location of our VSs, the ice juxtaposing (and consequently the ice bottom roughness) is unimportant. Future investigations with dedicated in-situ observations on river ice texture evolution are needed to understand the effect of bottom roughness on radar altimeter return signals.

Ice internal layering is also important for the scattering of radar signals (Legrésy et al., 1997; Nilsson et al., 2015; Slater et al., 2019). Under the climate conditions of northwestern Siberia, ice layering (characterised by dense

595 reflective icy surfaces) is rare, as the air temperature of winter warming episodes never approaches the melting point. Daily positive temperatures lasting several hours can occur starting from the end of March in the southern part of the study area and 1-2 weeks later to the north. During this time of the year, the ice was well developed and almost reached its maximum thickness. Layering can also occur after river water floods the ice surface through cracks. According to in-situ observations at gauging stations, this phenomenon was observed in the last several years
600 at the end of the ice season in the southern part of the study area. Both warming episodes and flooding events lead to a backscatter increase in the order of 1-5 dB and make altimetric ice thickness retrievals difficult by the end of the ice season. The highest underestimation of Hice (0.15-0.20 m) was observed in such cases.

The internal ice structure can also affect the backscatter value, for example, via air bubble inclusion (Gunn et al., 2018). During ice formation, jamming and ridging, can occur in Arctic rivers, resulting in the formation of air
605 pockets. Ridging is rare near gauging stations on the Ob River. However, there is no information about the state of the ice at other ungauged reaches, including the areas covered by VSs. We can only speculate that ridging/hummocking could be one of the reasons for the high difference in the coefficients of equation (3) determined for VS109 and for the lower accuracy of the Hice retrievals at this station compared to the northern virtual stations. On Landsat-8 images acquired for two springs in 2019/04/25 and 2015/05/01 (not shown), the
610 irregular spatial ice structure in the area of VS109 indirectly confirms our hypothesis. More studies involving the simultaneous analysis of SAR imagery showing ice field irregularities (Unterschultz et al., 2009) and altimetric signals could help to clarify this issue.

7.2 Potential improvements of algorithms

615 Results obtained demonstrate that the altimetric retrievals of ice phenology dates and thickness are able to capture the interannual variability of these parameters and can potentially be used in climate studies (see Figures 7 and 10a). In spite of the potential for climate change monitoring, we cannot recommend the use of the current (prototype) version of the ice thickness altimetric product for winter road opening forecasts, as it seems that for many locations we overestimate the thickness at the beginning of the freeze-up period (see Figure 10b). The inaccurate detection of
620 ice onset can affect the accuracy of ice thickness estimates, especially at the beginning of freeze-up. Another reason of uncertainties is the multi-peak character of the backscatter winter recession curve and the residual noise that could remain in the backscatter time series after the application of the LOESS filter. This occurred, for example, at VS12 where a polynya persisted until March in at least four years of the study period, producing a noisy recession curve (see Figure 3a) and a high dispersion of points around the 1:1 relation line on the Halti - Hinsitu scatterplot
625 (Figure 9).

Several improvements are proposed for future studies. First, an improvement in the accuracy of detection of the freeze-up algorithm is envisaged. In our algorithm, the ice thickness estimation starts from the date of the first ice (bank ice or frazil ice floes) appearance. Usually, river reaches in the area of the VSs at this time of the year are not fully frozen. The detection of the date of the first consolidated ice (i.e. fully frozen reaches) may help to reduce the
630 errors in the retrievals in a low range of ice thickness. A second improvement would involve the use of other parameters of the altimetric radar waveform instead of (or in complement to) the backscatter coefficient. As shown in Figure 3b, the main peak of the radar waveform decreases as ice grows. We suggest that the amplitude of the main peak or the area under this peak may produce stronger relationships with in-situ ice observations than the backscatter coefficient alone. During winter, the main peak is the most variable part of the waveform. This peak
635 corresponds to the return signals from the ice bottom (Beckers et al., 2017). The other part of the waveform records

the return signal from the surrounding (off-nadir) areas and also contributes to the total value of the backscatter coefficient. Any temporal changes in the state of surrounding areas that are different from the state in the near-nadir area (e.g. ice flooding or off-nadir polynya) lead to backscatter changes not related to ice growth. Consequently, the use of waveform parameters related to the main peak could reduce the errors in ice thickness estimates. Unfortunately, these parameters are not directly provided in the AVISO+ Jason GDR product, but they could potentially be estimated from the initial waveforms.

7.3 Potential application of radar altimetry to other rivers

One of the main advantages of satellite altimetry compared to imaging SAR relates to the relative ease in processing their measurements over the large hemispheric-scale domain. As the developed ice phenology dates algorithm is independent of the availability of in-situ observations, it can be directly applied to other rivers. The main limitation of algorithm would be the width of the river, which, from our experience, is limited by 100-200 m. The algorithm can be also applied to lakes and bogs, as the temporal variability of the backscatter over these surfaces is similar to that described in the section 3. However, the algorithm would need an additional adjustment/verification for rivers with unstable winter ice cover, at mid latitudes for example, as well as in areas of frequent occurrence of rain-on-snow/ice episodes.

Unfortunately, similar to the proposed imaging SAR-based methods (Unterschultz et al., 2009; Mermoz et al., 2014), the availability of ground truth data is indispensable for our ice thickness retrieval algorithm. Nevertheless, we demonstrated that for the sufficiently long river reaches the obtained empirical relations between in-situ data and satellite measurements are quite close to each other. We suggest that the use of $\Delta Sig0/\Delta t$, instead of the absolute value of Sig0, allows for minimisation of the perturbing effect of surrounding banks (i.e. local morphological conditions). The character of the surrounding banks affects the backscatter values at the beginning of the freeze-up period (i.e. ice onset). The effect of the initial ice conditions was thus reduced. The unification of the relations and its application to other reaches and other rivers is likely possible when using $\Delta Sig0/\Delta t$. However, further investigations are needed to assess the impact of ice texture/type on parameters of the retrieval equation. Hence, the combination of data from imaging SAR (providing information on ice type) and altimetric satellite missions could be beneficial.

8 Conclusion

The decreasing number of in-situ observation sites and degradation of the quality of their time series is a good argument for furthering the development of satellite remote sensing methods for freshwater ice monitoring. The present study demonstrates for the first time the potential of satellite radar altimetry for monitoring river ice parameters such as freeze-up, breakup, and ice thickness for the large Arctic Ob River.

An algorithm based on the analysis of backscatter coefficients from the Jason-2 and -3 satellite altimeters provides an estimation of river ice onset with an accuracy of ±10 days (corresponding to the 10-day satellite overpass frequency) in 90% of the cases. River ice breakup consists of two phases: thermal degradation and mechanical breakup. The algorithm can detect the beginning of thermal degradation well with the same accepted accuracy of ±10 days for 88% of the cases. River ice thickness was retrieved from altimetric backscatter measurements via simple empirical relations with in-situ observations. The accuracy of the thickness retrievals (expressed as RMSE) ranges from 0.07 to 0.18 m.

Spatio-temporal interpolation and smoothing of satellite-derived river ice thickness retrieved for 48 VSs along the 400 km reaches of the Lower Ob River allowed for the elaboration of weekly maps generalised in the form of an annual spatio-temporal product. The ice thickness time series can be extracted for any location and used for climate change monitoring and ice road operational purposes. Using this first version of the product, we showed that the dates of opening of the ice road near Salekhard City can be predicted from altimetric ice onset retrievals with an accuracy of four days. Errors in the prediction of dates of ice road closure were within three days. Despite these promising results, we consider that the current (prototype) version of the product is not sufficiently mature for operational use as it overestimates ice thickness at the beginning of the ice season. The accurate estimation of ice thickness is critical for safety. However, the algorithm and product could be significantly improved in the future through a multi-mission and multi-instrument (optical and/or SAR imagers) approach. We are confident that with the use of the Copernicus satellite altimeters Sentinel-3A and 3B, an improvement in the retrieval of ice thickness can be made. These satellite missions carry more advanced altimetric SAR instruments with footprints representing a narrow band and return signals that are less contaminated by land than signals from the conventional Jason instrument. Although the nominal repeat frequency of the Sentinel-3 satellites (27 days) is not suitable for operational applications, they provide five overpasses within a 25 km distance around the Salekhard City ice road and, thus, the temporal resolution of observations may be significantly improved. The combination of data from the Jason and Sentinel-3 missions could be fruitful.

The Salekhard ice road is very well instrumented, monitored, and maintained by local authorities, thanks to the high demand for its use and high merchandise flow. In other regions, ice roads connecting small cities and villages are less monitored, and access to operational information is poor. Moreover, many intermittent and unofficial river crossings are developed each year by local people. Often, the lack of information on the state of ice results in accidents and requires intervention by the emergency service. The demonstrated capability of the first version of the altimetric river ice product as a supporting tool for the ice road operation on the Ob River is quite promising. Further product improvements and the development of sophisticated prediction criteria for road operation that could be adapted to other reaches of the Ob River are planned.

Acknowledgements. The authors express their gratitude to the staff of the State Traffic Service of Yamalo-Nenetzky Autonomous District (Russia) for providing the valuable information about ice road operation. The authors would also like to thank the two anonymous referees for their thorough and constructive comments.

Funding. This research was made possible with support from RFBR project No. 18-05-60021-Arctic, ESA (EO Science for Society Element) LIAM project (Contract No. 4000130930/20/I-DT) and ESA CCI Lakes+ (Contract No. 4000125030/18/I-NB –CCI+ PHASE1 – NEW ECVS - Lakes); the approbation of results was carried out in the framework of Governmental Program of Water Problems Institute, Russian Academy of Sciences, No. 0147-2019-0004.

Author contribution. All authors contributed to the data collection, algorithm development, analysis and presentation of results equally.

Declaration of Interests. The authors declare no competing interests.

References

Agafonova, S.A., and Vasilenko, A.N.: Hazardous ice phenomena in rivers of the Russian arctic zone under current climate conditions and the safety of water use, Geography, Environment, Sustainability, 13, 2: 43–51, doi.org/10.24057/2071-9388-2020-12, 2020.

Atwood, D. K., Gunn, G. E., Roussi, C., Wu, J., Duguay, C.R., and Sarabandi, K.: Microwave backscatter from Arctic lake ice and polarimetric implications, IEEE Transactions on Geosciences and Remote Sensing, 53, 11: 5972–5982, doi:10.1109/TGRS.2015.2429917, 2015.

Antonova, S., Duguay, C.R., Kääb, A., Heim, B., Langer, M., Westermann, S., and Boike, J.: Monitoring ice phenology and bedfast ice in lakes of the Lena River Delta using TerraSAR-X backscatter and coherence time series, Remote Sensing, 8(11): 903, doi:10.3390/rs8110903, 2016.

Bamber, J. L.: Ice sheet altimeter processing scheme, International Journal of Remote Sensing, 15, 4: 925 – 938, doi.org/10.1080/01431169408954125, 1994.

Beaton, A., Whaley, R., Corston, K., and Kenny, F.: Identifying historic river ice breakup timing using MODIS and Google Earth Engine in support of operational flood monitoring in Northern Ontario, Remote Sensing of Environment, 224: 352–364, doi.org/10.1016/j.rse.2019.02.011, 2019.

Beckers J. F., Casey, J.A., and Haas, C.: Retrievals of lake ice thickness from Great Slave Lake and Great Bear Lake using CryoSat-2, IEEE Transactions on Geoscience and Remote Sensing, 55, 7: 3708-3720, doi: 10.1109/TGRS.2017.2677583, 2017.

Beltaos, S.: Hydrodynamic characteristics and effects of river waves caused by ice jam releases, Cold Regions Science and Technology 85: 42–55, dx.doi.org/10.1016/j.coldregions.2012.08.003, 2013.

Beltaos S., Carter T., Rowsell R., and DePalmac S.G.S.: Erosion potential of dynamic ice breakup in Lower Athabasca River. Part I: Field measurements and initial quantification, Cold Regions Science and Technology, 149: 16-28, doi.org/10.1016/j.coldregions.2018.01.013, 2018.

Berry, P. A. M., Garlick, J. D., Freeman, J. A., and Mathers, E. L.: Global inland water monitoring from multi-mission altimetry, Geophysical research letter 32: L16401, doi: 10.1029/2005GL022814, 2005.

Brown G.S.: The average impulse response of a rough surface and its applications. IEEE Journal of Ocean Engineering, 2 : 67-74, 10.1109/JOE.1977.1145328, 1977.

Chaouch, N., Temimi, M., Romanov, P., Cabrera, R., McKillop, G., and Khanbilvardi, R.: An automated algorithm for river ice monitoring over the Susquehanna River using the MODIS data, Hydrological Processes, 28: 62–73, doi.org/10.1002/hyp.9548, 2014.

Chu, T. and Lindenschmidt, K.-E.: Integration of space-borne and air-borne data in monitoring river ice processes in the Slave River, Canada, Remote Sensing of Environment, 181: 65-81, doi.org/10.1016/j.rse.2016.03.041, 2016.

Cooley, S. W. and Pavelsky, T.M.: Spatial and temporal patterns in Arctic river ice breakup revealed by automated ice detection from MODIS imagery, Remote Sensing of Environment. 175: 310–322, doi.org/10.1016/j.rse.2016.01.004, 2016.

Du, J., Kimball, J.S., Duguay, C.R., Kim, Y., and Watts, J.: Satellite microwave assessment of Northern Hemisphere lake ice phenology from 2002 to 2015, The Cryosphere, 11: 47–63, doi:10.5194/tc-11-47-2017, 2017.

Duguay, C.R., Bernier, M., Gauthier, Y., and Kouraev, A.: Remote sensing of lake and river ice. In Remote Sensing of the Cryosphere, Edited by M. Tedesco. Wiley-Blackwell (Oxford, UK), 273-306, ISBN-13:978-1118368855, 2015.

Duguay, C.R., Pultz, T.J., Lafleur, P.M., and Drai, D.: RADARSAT backscatter characteristics of ice growing on shallow sub-arctic lakes, Churchill, Manitoba, Canada, Hydrological Processes, 16, 8: 1631-1644, doi: 10.1002/hyp.1026, 2002.

Duguay, C.R., Zakharova, E.A., Kouraev, A.V., Kheyrollah Pour, H., and Hoekstra, M.: Retrieval of ice thickness on large northern lakes from Jason-2 data, POLAR2018: Abstract Proceedings, Open Science Conference, Davos, Switzerland, 19-23 June, Abstract No. 2638, p. 46, 2018.

ESA: ENVISAT RA2/MWR Product Handbook, RA2/MWR Products User Guide, 2002.

Ettema, R.: Review of alluvial-channel responses to river ice, Journal of Cold Regions Engineering, 16: 191–217, doi.org/10.1061/(ASCE)0887-381X(2002)16:4(191), 2002.

Fu L.-L., and Cazenave A.: Satellite Altimetry and Earth Sciences: A Handbook of Techniques and Applications, Elsevier, Nov 9, 2000: 463, ISBN0080516580, 9780080516585, 1991.

Ginzburg, B.M.: Probabilistic characteristics of freeze-up and breakup dates on rivers and reservoirs of the Soviet Union. Leningrad, Hydrometeoizdat, 110p., 1973.

Guerreiro K., Fleury, S., Zakharova, E., Rémy, F., and Kouraev, A.: Potential for estimation of snow depth on Arctic sea ice from CryoSat-2 and SARAL/AltiKa missions, Remote Sensing of Environment, 186: 339-349, https://doi.org/10.1016/j.rse.2016.07.013, 2016.

Gunn G. E., Duguay, C. R., Brown, L. C., King, J. M. L., Atwood, D., and Kasurak, A.: Freshwater lake ice thickness derived using surface-based X- and Ku-band FMCW scatterometers, Cold Regions Science and Technology,120: 115–126, doi.org/10.1016/j.coldregions.2015.09.012, 2015.

Gunn, G.E., Duguay, C.R., Atwood, D.K., King, J., and Toose, P.: Observing scattering mechanisms of bubbled freshwater lake ice using polarimetric RADARSAT-2 (C-band) and UW-Scat (X- and Ku-bands), IEEE Transactions on Geoscience and Remote Sensing, 56, 5, doi: 10.1109/TGRS.2017.2786158 , 2018.

Instructions on Safety Organisation of rivers' and lakes' crossing, RD 34.03.221, INFORMENRGO, Moscow, 1969.

Jeffries M.O. , Morris, K., and Kozlenko, N.: Chapter 4 - ice characteristics and processes, and remote sensing of frozen Rivers and lakes. C.R. Duguay, A. Pietroniro (Eds.), Remote Sensing in Northern Hydrology: Measuring Environmental Change, American Geophysical Union, Washington, DC : 63-90, ISBN-13:978-0-87590-428-3, 2005.

Kang K.-K., Duguay, C.R., Lemmetyinen, J., and Gel, Y.: Estimation of ice thickness on large northern lakes from AMSR-E brightness temperature measurements, Remote Sensing of Environment, 150: 1-19, doi.org/10.1016/j.rse.2014.04.016, 2014.

Kang, K-K., Duguay, C. R., and Howell, S. E. L.: Estimating ice phenology on large northern lakes from AMSR-E: Algorithm development and application to Great Bear Lake and Great Slave Lake, Canada, The Cryosphere, 6: 235-254, doi:10.5194/tc-6-235-2012, 2012.

Kheyrollah Pour, H., Duguay, C.R., Scott, A., and Kang, K.-K.: Improvement of lake ice thickness retrieval from MODIS satellite data using a thermodynamic model, IEEE Transactions on Geoscience and Remote Sensing, 55, 10: 5956-5965, doi: 10.1109/TGRS.2017.2718533, 2017.

King, J.M.L., Kelly, R., Kasurak, A., Duguay, C., Gunn, G., and Mead, J.B.: UW-Scat - ground-based dual frequency scatterometry for observation of snow processes, IEEE Geoscience and Remote Sensing Letters, 10, 3: 528-532, doi: 10.1109/LGRS.2012.2212177, 2013.

King, J.M.L., Kelly, R., Kasurak, A., Duguay, C., Gunn, G., Rutter, N., Watts, T., and Derksen, C.: Spatio-temporal influence of tundra snow properties on Ku-band (17.2 GHz) backscatter, Journal of Glaciology, 61, 226: 267-279, doi: 10.3189/2015JoG14J020, 2015.

Kouraev, A.V., Zakharova, E.A., Samain, O., Mognard, N.M., and Cazenave, A.: Ob' River discharge from TOPEX/Poseidon satellite altimetry (1992–2002), Remote Sensing of Environment, 93, 1: 238–245, doi.org/10.1016/j.rse.2004.07.007, 2005.

Kouraev, A.V., Zakharova, E.A., Rémy, F., and Suknev, A.Y.: Study of Lake Baikal ice cover from radar altimetry and in situ observations, Marine Geodesy, Special issue on SARAL/AltiKa, 38 (sup1): 477-486, doi.org/10.1080/01490419.2015.1008155, 2015.

Kouraev, A.V., Semovski, S.V., Shimaraev, M., Mognard, N.M., Legrésy, B., and Rémy F.: Observations of Lake Baikal ice from satellite altimetry and radiometry, Remote Sensing of Environment, 108: 240–253, doi.org/10.1016/j.rse.2006.11.010, 2007.

Kurtz, N. T., Galin, N., and Studinger, M.: An improved CryoSat-2 sea ice freeboard retrieval algorithm through the use of waveform fitting, The Cryosphere, 8: 1217–1237, https://doi.org/10.5194/tc-8-1217-2014, 2014.

Leconte, R, Daly, S., Gauthier, Y., Yankielun, N., Bérubé, F., and Bernier, M.: A controlled experiment to retrieve freshwater ice characteristics from an FM-CW radar system, Cold Regions Science and Technology, 55, 2: 212–220, 2009.

Larue, F., Picard, G., Aublanc, J., Arnaud, L., Robledano-Perez, A., Le Meur, E., Favier, V., Jourdain, B., Savarino, J., and Thibaut, P.: Radar altimeter waveform simulations in Antarctica with the Snow Microwave Radiative Transfer Model (SMRT), Remote Sensing of Environment, 263, doi:10.1016/j.rse.2021.112534, 2021.

Legrésy, B., and Rémy, F.: Surface characteristics of the Antarctic ice sheet and altimetric observations, Journal of Glaciology, 43, 14: 265−275, doi.org/10.3189/S002214300000321X, 1997.

Mermoz, S., Allain, S., Bernier, M., and Pottier, E.: Investigation of Radarsat-2 and TerraSAR-X data for river ice classification, IEEE International Geoscience and Remote Sensing Symposium, Cape Town, II-29-II-32, doi: 10.1109/IGARSS.2009.5417991, 2009.

Mermoz S., Allain-Bailhache, S., Bernier, M., Pottier, E., van der Sanden, J.J., and Chokmani, K.: Retrieval of river ice thickness from C-band PolSAR data, IEEE Transactions on Geoscience and Remote Sensing, 52, 6: 3052-3062, doi: 10.1109/TGRS.2013.2269014, 2014.

Michailovsky, C. I., McEnnis, S., Berry, P. A. M., Smith, R., and Bauer-Gottwein, P.: River monitoring from satellite radar altimetry in the Zambezi river basin, Hydrology and Earth System Science, 16, 7: 2181–2192, doi:10.5194/hess-16-2181-2012, 2012.

Morse, B. and Hicks, F.: Advances in river ice hydrology 1999–2003, Hydrological Processes, 19: 247–263, doi: 10.1002/hyp.5768, 2005.

Muhammad, P., Duguay, C.R., Kang, K.-K.: Monitoring ice break-up on the Mackenzie River using remote sensing, The Cryosphere, 10: 569-584, doi:10.5194/tc-10-569-2016, 2016.

Murfitt, J. and Duguay, C.R.: 50 years of lake ice research from active microwave remote sensing: Progress and prospects, Remote Sensing of Environment, 264: 112616, https://doi.org/10.1016/j.rse.2021.112616, 2021.

Nilsson, J., Vallelonga, P., Simonsen, S.B., Sorensen, L.S., Forsberg, R., Dahl-Jensen, D., Hirabayashi, M., Goto-Azuma, K., Hvidberg, C.S., Kjaer, H.A., and Satow, K.: Greenland 2012 melt event effects on CryoSat-2 radar altimetry, Geophysical Research Letters, 42: 3919–3926, doi: 10.1002/2015GL063296, 2015.

Picard, R. and Cook, R.: Cross-validation of regression models, Journal of the American Statistical Association, 79: 575–583, doi.org/10.2307/2288403, 1984.

Pavelsky, T. M. and Smith, L. C.: Spatial and temporal patterns in Arctic river ice breakup observed with MODIS and AVHRR time series, Remote Sensing of Environment, 93: 328–338, doi:10.1016/j.rse.2004.07.018, 2004.

Prowse, T.D.: River-ice ecology: part B. Biological aspects, Journal of Cold Regions Engineering 15: 17–33, doi.org/10.1061/(ASCE)0887-381X(2001)15:1(17), 2001.

Prowse, T., Alfredsen, K., Beltaos, S., Bonsal, B., Duguay, C., Korhola, A., McNamara, J., Pienitz, R., Vincent, W.F., Vuglinsky, V., and Weyhenmeyer, G.A.: Past and future changes in Arctic lake and river ice, AMBIO, 40: 53–62, doi: 10.1007/s13280-011-0216-7, 2011a.

Prowse, T., Alfredsen, K., Beltaos, S., Bonsal, B., Bowden, W., Duguay, C., Korhola, A., McNamara, J., Vincent, W.F., Vuglinsky, V., Anthony, K., and Weyhenmeyer, G.A.: Effects of changes in Arctic lake and river ice, AMBIO 40: 63–74, doi.org/10.1007/s13280-011-0217-6, 2011b.

Prowse, T.D., Bonsal, B.R., Duguay, C.R., and Lacroix, M.P.: River-ice break-up/freeze-up: A review of climatic drivers, historical trends, and future predictions, Annals of Glaciology, 46: 443-451, 2007.

Rémy, F., Flament, T., Blarel, F., Benveniste, J.: Radar altimetry measurements over Antarctic ice sheet: a focus on antenna polarization and change in backscatter problems, Advances in Space Research, 50 : 998-1006, 10.1016/j.asr.2012.04.003, 2012.

Slater, T., Shepherd, A., McMillan, M., Armitage, T. W. K., Otosaka, I., and Arthern, R. J.: Compensating changes in the penetration depth of pulse-limited radar altimetry over the Greenland ice sheet, IEEE Transactions on Geoscience and Remote Sensing, 57, 12: 9633-9642, doi: 10.1109/TGRS.2019.2928232, 2019.

Sobiech, J. and Dierking, W.: Observing lake- and river-ice decay with SAR: advantages and limitations of the unsupervised k-means classification approach, Ann. Glaciol., 54: 65–72, doi:10.3189/2013AoG62A037, 2013.

Sun, W. and Trevor, B.: A stacking ensemble learning framework for annual river ice breakup dates, Journal of Hydrology, 561: 636-650. doi.org/10.1016/j.jhydrol.2018.04.008. 2018.

Ulaby, F. T., Moore, R. K. , and Fung, A. K.: Microwave Remote Sensing: Active and Passive, Radar Remote Sensing and Surface Scattering and Emission Theory, vol. 2. Norwood, MA, USA: Addison-Wesley, 1986.

Unterschultz, K., van der Sanden, J., and Hicks, F.: Potential of RADARSAT-1 for the monitoring of river ice: Results of a case study on the Athabasca River at Fort McMurray, Canada, Cold Regions Science and Technology, 55: 238–248, doi:10.1016/j.coldregions.2008.02.003, 2009.

van der Sanden J., Drouin, H., and Geldsetzer, T.: An automated procedure to map breaking river ice with C-band HH SAR data, Remote Sensing of Environment, 252: 112119, https://doi.org/10.1016/j.rse.2020.112119, 2021.

Vuglinsky, V. and Valatin, D.: Changes in ice cover duration and maximum ice thickness for rivers and lakes in the Asian part of Russia, Natural Resources, 9: 73-87. https://doi.org/10.4236/nr.2018.93006, 2018.

Willatt, R., Laxon, S., Giles, K., Cullen, R., Haas, C., and Helm, V.: Ku-band radar penetration into snow cover on Arctic sea ice using airborne data, Annals of Glaciology, 52, 57: 197–205, doi.org/10.3189/172756411795931589 2011.

Zakharova, E.A., Kouraev, A.V., Rémy, F., Zemtsov, V.A., and Kirpotin, S.N.: Seasonal variability of the Western Siberia wetlands from satellite radar altimetry, Journal of Hydrology, 512: 366–378. doi.org/10.1016/j.jhydrol.2014.03.002, 2014.

Zakharova E.A., Krylenko, I.N., and Kouraev, A.V.: Use of non-polar orbiting satellite radar altimeters of the Jason series for estimation of river input to the Arctic Ocean, Journal of Hydrology, 568: 322-333, doi.org/10.1016/j.jhydrol.2018.10.068, 2019.

Zakharova, E,A., Nielsen, K., Kamenev, G., and Kouraev, A.: River discharge estimation from radar altimetry: Assessment of satellite performance, river scales and methods, Journal of Hydrology, 583: 124561, doi.org/10.1016/j.jhydrol.2020.124561, 2020.

Zhang, F., Li, Z., and Lindenschmidt, K.-E.: Potential of RADARSAT-2 to improve ice thickness calculations in remote, poorly accessible areas: A case study on the Slave River, Canada, Canadian Journal of Remote Sensing, 45(2): 234-245, doi: 10.1080/07038992.2019.1567304, 2019.